Experimental Neurology 317 (2019) 51–65

Contents lists available at ScienceDirect

Experimental Neurology

journal homepage: www.elsevier.com/locate/yexnr

Research paper

Free D-aspartate triggers NMDA receptor-dependent cell death in primary cortical neurons and perturbs JNK activation, Tau phosphorylation, and protein SUMOylation in the cerebral cortex of mice lacking D-aspartate oxidase activity

Tommaso Nuzzo[a,1], Marco Feligioni[b,c,1], Luigia Cristino[d,1], Ilaria Pagano[e,1], Serena Marcelli[f], Filomena Iannuzzi[c], Roberta Imperatore[f], Livia D'Angelo[g,h], Carla Petrella[i], Massimo Carella[a], Loredano Pollegioni[j], Silvia Sacchi[j], Daniela Punzo[k,l], Paolo De Girolamo[g], Francesco Errico[m], Nadia Canu[e,n,**], Alessandro Usiello[k,l,*]

[a] Translational Neuroscience Unit, IRCCS Casa Sollievo della Sofferenza, 71013, San Giovanni Rotondo, Italy
[b] Laboratory of Neuronal Cell Signaling, EBRI Rita Levi-Montalcini Foundation, Rome, Italy
[c] Neurobiology in Translational Medicine, Department of Neurorehabilitation Sciences, Casa Cura Policlinico, Milan, Italy
[d] Institute of Biomolecular Chemistry (I.C.B.), National Research Council (C.N.R.), 80078, Pozzuoli, Naples, Italy
[e] Institute of Cell Biology and Neurobiology, 00015, Monterotondo Scalo, Rome, Italy
[f] Department of Sciences and Technologies, University of Sannio, 82100, Benevento, Italy
[g] Department of Veterinary Medicine and Animal Productions, University of Naples Federico II, Naples, Italy
[h] Stazione Zoologica Anton Dohrn, Naples, Italy
[i] Institute of Cell Biology and Neurobiology/CNR, Department of Sense Organs, Sapienza University of Rome, Italy
[j] Department of Biotechnology and Life Sciences, University of Insubria, 21100, Varese, Italy
[k] Department of Environmental, Biological and Pharmaceutical Sciences and Technologies, University of Campania Luigi Vanvitelli, 81100, Caserta, Italy
[l] Laboratory of Behavioural Neuroscience, Ceinge Biotecnologie Avanzate, 80145, Naples, Italy
[m] Department of Agricultural Sciences, University of Naples "Federico II", 80055, Portici, Italy
[n] Department of System Medicine, University of Rome "Tor Vergata", 00137, Rome, Italy

ARTICLE INFO

Keywords:
D-aspartate
D-aspartate oxidase
NMDA receptor
Aging
JNK
Tau
SUMOylation
β-Amiloyd
Alzheimer's disease
Mouse models

ABSTRACT

In mammals, free D-aspartate (D-Asp) is abundant in the embryonic brain, while levels remain very low during adulthood as a result of the postnatal expression and activity of the catabolizing enzyme D-aspartate oxidase (DDO). Previous studies have shown that long-lasting exposure to nonphysiological, higher D-Asp concentrations in *Ddo* knockout ($Ddo^{-/-}$) mice elicits a precocious decay of synaptic plasticity and cognitive functions, along with a dramatic age-dependent expression of active caspase 3, associated with increased cell death in different brain regions, including hippocampus, prefrontal cortex, and substantia nigra *pars compacta*. Here, we investigate the yet unclear molecular and cellular events associated with the exposure of abnormally high D-Asp concentrations in cortical primary neurons and in the brain of $Ddo^{-/-}$ mice. For the first time, our *in vitro* findings document that D-Asp induces in a time-, dose-, and NMDA receptor-dependent manner alterations in JNK and Tau phosphorylation levels, associated with pronounced cell death in primary cortical neurons. Moreover, observations obtained in $Ddo^{-/-}$ animals confirmed that high *in vivo* levels of D-Asp altered cortical JNK signaling, Tau phosphorylation and enhanced protein SUMOylation, indicating a robust indirect role of DDO activity in regulating these biochemical NMDA receptor-related processes. Finally, no gross modifications in D-Asp concentrations and *DDO* mRNA expression were detected in the cortex of patients with Alzheimer's disease when compared to age-matched healthy controls.

* Correspondence to: A. Usiello, Ceinge Biotecnologie Avanzate, Via G. Salvatore, 486, 80145 Naples, Italy.
** Correspondence to: N. Canu, Department of System Medicine, University of Rome "Tor Vergata", Via Montpellier 1, 00133 Rome, Italy.
E-mail addresses: nadia.canu@uniroma2.it (N. Canu), usiello@ceinge.unina.it (A. Usiello).
[1] These authors contributed equally to this work.

https://doi.org/10.1016/j.expneurol.2019.02.014
Received 30 December 2018; Received in revised form 19 February 2019; Accepted 24 February 2019
Available online 26 February 2019
0014-4886/

1. Introduction

Free D-aspartate (D-Asp) is abundant in the embryonic brain of mammals (Hashimoto et al., 1993; Homma, 2007). As a result of the postnatal expression and activity of the catabolizing enzyme D-aspartate oxidase (DDO), the levels of this D-amino acid substantially decrease from the first weeks of life and remain very low during adulthood (Homma, 2007; Punzo et al., 2016; Schell et al., 1997; Van Veldhoven et al., 1991). Recent *in vivo* microdialysis experiments showed that D-Asp is also present in the extracellular space (Guida et al., 2015; Punzo et al., 2016; Sacchi et al., 2017), where it binds to the agonist site of NMDA receptors (NMDARs) (Fagg and Matus, 1984; Monahan and Michel, 1987; Ogita and Yoneda, 1988; Olverman et al., 1988; Ransom and Stec, 1988) and activates this receptor subclass (Errico et al., 2011a; Errico et al., 2011b; Errico et al., 2008; Krashia et al., 2016). In addition to its direct postsynaptic effect on NMDARs, experiments performed on mouse cortical synaptosomes have recently demonstrated that D-Asp also stimulates presynaptic NMDA, AMPA, and mGluR receptors, in turn triggering the *in vivo* release of L-glutamate (L-Glu) as measured by microdialysis in the cortex of freely moving mice (Cristino et al., 2015; Sacchi et al., 2017). Thus, in line with the detrimental effects produced by dysfunctional stimulation of glutamatergic transmission at NMDARs (Hardingham and Bading, 2003; Waxman and Lynch, 2005), our studies have previously shown that long-lasting exposure to nonphysiological, higher D-Asp concentrations dramatically accelerates the rate of age-dependent brain deterioration processes. Consistently, in *Ddo* knockout ($Ddo^{-/-}$) mice, the lack of DDO activity triggers an abnormally precocious decay of NMDAR-dependent hippocampal functions, including long-term potentiation (LTP) (Cristino et al., 2015; Errico et al., 2011a; Errico et al., 2011b) and spatial learning and memory (Errico et al., 2011a; Errico et al., 2011b). Remarkably, these functional impairments are mirrored overall by enhanced age-dependent expression of active caspase 3 and 7 and increased cell death in the hippocampus of $Ddo^{-/-}$ mice as early as 6 months of age (Cristino et al., 2015). As in the hippocampus, precocious caspase activation and apoptosis occur in the prefrontal cortex (PFC) and substantia nigra of $Ddo^{-/-}$ brains, too (Punzo et al., 2016). Furthermore, we observed an early accumulation of lipofuscin in the brain of $Ddo^{-/-}$ animals (Punzo et al., 2016), thus suggesting that persistent levels of D-Asp elicit a greater activation of oxidative stress pathways, likely mediated by NMDAR overstimulation. In line with these observations, we also reported severe neuroinflammation processes, as demonstrated by the appearance of dystrophic microglia and reactive astrocytes in these mutants (Cristino et al., 2015; Punzo et al., 2016). Taken together, these data indicate that a lack of DDO activity triggers a dysfunctional NMDAR transmission, which results in the structural and functional manifestations typical of neurodegenerative forms of dementia (Mitchell et al., 2015). Despite this knowledge, the signal transduction pathways underlying the neurotoxicity processes induced by persistently deregulated high levels of D-Asp still remain elusive. In the present study, therefore, we first explored the molecular and cellular consequences of increased free D-Asp concentrations in cortical primary neurons. Then, we investigated whether abnormally elevated levels of D-Asp in $Ddo^{-/-}$ prefrontal cortex are linked to the emergence of pathological phenotypes resembling those specifically reported in animal models of Alzheimer's disease (AD) (Hall and Roberson, 2012). Finally, D-Asp levels and *DDO* mRNA expression in the cortex of patients with AD were also analyzed *postmortem*.

2. Materials and methods

2.1. Primary neuronal cells

Cortical cultures were prepared from embryo brains at day 17/18 (E17/E18) from timed pregnant Wistar rats (Charles River), as previously reported (Amadoro et al., 2006). In brief, cortex was dissected out in Hanks' balanced salt solution buffered with Hepes and dissociated *via* trypsin treatment. Cells were plated in 24-well dishes precoated with poly-Lysine (Sigma Aldrich, St. Louis, MO). The cultures were plated in neurobasal medium (Gibco, Milan, Italy) supplemented with B27 (2%; Gibco), L-glutamine (0.5 mM), and antibiotic penicillin/streptomycin (1%). After 2 days, half of the medium D-Asp was added to the culture medium at different concentrations for the time indicated: MK801 (10 μM), Ifenprodil (IFP, 10 μM) and 3-[(2-methyl-1,3-thiazol-4-yl)ethynyl]pyridine (MTEP, 5 μM were added 30 min before and throughout the period of NMDA treatment.

2.2. Assessment of cell viability

Viability was quantified by the 4,5-dimethylthiazol-2-yl)-2,5-diphenyltetrazolium bromide (MTT) assay (Esposito et al., 2012) and by lactate dehydrogenase release assay (Van Veldhoven et al., 1991). The LDH release assay was performed to assess cell death by measuring the release of LDH into the medium from damaged cells due to necrosis or secondary necrosis following apoptosis. Culture medium (50 μL) was collected after treatment with D-Asp from the different groups. An equivalent volume (50 μL) of detection reagent (LDH-Cytotoxicity Colorimetric Assay Kit Catalog #: K311. BioVision USA) was added to each well containing the culture medium and incubated for 30 min in the dark at room temperature. The absorbance was measured (wavelength = 490 nm) using a colorimetric microplate reader (EnSpire multimode plate reader, Perkin Elmer). Three replicates for each time point per experiment were assayed, and three such experiments were performed.

2.3. Fluorogenic peptide substrate assay for caspase-3 activity

Caspase-3 activity was measured, as described previously (Esposito et al., 2012). After different times of D-aspartate treatment (10 μM and 100 μM) and in the absence or presence of MK801 (10 μM), cortical neurons were washed once with PBS and lysed in 100 μl of buffer A (10 mM HEPES pH 7.4, 42 mM KCl, 5 mM MgCl2, 1 mM dithio-threitol (DTT), and 1 mM PMSF, 0.5% 3-[(3-cholamidopropyl) dimethylammonio]-1-propanesulphonic acid (CHAPS), and 1 mg/ ml leupeptin). Lysate (25 μl) was combined with 75 μl of buffer B (25 mM HEPES, 1 mM EDTA, 0.1% CHAPS, 10% sucrose, and 3 mM DTT, pH 7.5) containing Ac-DEVD-MCA (30 μM) and incubated for 20 min at 22 °C. Fluorescence was measured at an excitation of 380 nm and an emission of 460-nm wavelengths using a Fluorocount microplate reader (EnSpire multimode plate reader, Perkin Elmer).

2.4. Tissue preparation

Mice were killed at the indicated time points, and PFC and hippocampi were isolated and stored at −80 °C until use. The brain tissues were homogenized in ice-cold extraction buffer (20 mM Tris–HCl, pH 8, 100 mM NaCl, 1 mM EDTA, 1 mM dithiothreitol, 0.5% Triton X-100, 20 mM NaF, and 1 mM activated Na3VO 4) supplemented with protease inhibitor cocktail (Sigma Aldrich) using the disposable polypropylene homogenizers fitting into the tip of 1.5 ml Eppendorf tubes (E&K Scientific Products, CA, USA). The homogenates were centrifuged at 20,800 × *g* for 20 min at 4 °C, to remove insoluble debris. Concentration of total proteins in the supernatant was determined by Bio-Rad Protein Assay (Bio-Rad Laboratories, Hercules, CA, USA).

2.5. Sodium dodecyl sulfate-polyacrylamide gel electrophoresis and immunoblot analysis

Sodium dodecyl sulfate-polyacrylamide gel electrophoresis (SDS-PAGE) was performed according to Laemmli (Laemmli, 1970). The supernatants were mixed with equal volumes of 2× SDS sample loading buffer and heated at 95 °C for 5 min. Proteins were separated in

12% SDS-PAGE gels. After electrophoresis, the separated proteins were transferred to a 0.2-μm Protran nitrocellulose membrane (Whatman, Maidstone, UK). The membranes were blocked for 1 h in 5% (w/v) milk in Tris-buffered saline containing Tween 20 (TBST; 20 mM Tris–HCl, pH 7.4, 0.15 M NaCl, and 0.1% Tween 20), then incubated with primary antibody diluted in 5% (w/v) milk in TBST overnight at 4 °C, washed four times for 10 min in TBST, followed by incubation with donkey anti-mouse secondary antibody conjugated to horseradish peroxidase diluted in 5% (w/v) milk in TBST (dilution 1:5000; Jackson Immunoreserach) for 1 h at 25 °C, and washed four times with TBST for 4 min. Blots were developed with Pierce TM ECL Western Blotting Substrate (Thermo Fisher Scientific, Waltham, Massachusetts, USA). Several antibodies were used in this study. They include Tau 7.51 (kind gift of M. Novak) 1/10, and Tau5 (AHB0042, Thermo Fisher Scientific) 1/1000 to detect total tau. Tau-1 clone PC1C6 (MAB3420, Millipore, Billerica, Massachusetts, USA) 1/1000 to detect tau dephosphorylated serine sites at 195, 198, 199, and 202. PHF-1 (kind gift of V. Lee) 1/1000 to detect phosphorylated serine sites at 396 and 404. AT8 (MN1020 Thermo Fisher Scientific) 1/100, to detect phosphorylated serine sites at 202 and 205. AT270 (MN1070, Thermo Fisher Scientific) 1/1000, to detect phosphorylated threonine site 181. P231 (AS-55313, Anaspec, Fremont, CA, USA) 1/500, to detect phosphorylated threonine site at 231. P396 (44-72G, Thermo Fisher Scientific) 1/1000, to detect phosphorylated serine at 396 site. Pan-GSK-3β, 1/5000 and phospho-GSK-3β Ser9 1/1000; total ERK1/2 and phospho ERK1/2, 1/1000; total-AKT, 1/1000, phospho-AKT Ser473, 1.1000, and cleaved caspase-3 (Asp175) antibodies were from Cell Signaling Technologies, Boston, MA, USA.

The p35 Cdk5 regulator (also recognizes p25, the truncated fragment of p35), 1/1000, and β-actin-HRP, 1/20000 were from Sigma Aldrich, St Louis, MO, USA) 1/1000, rabbit anti-SUMO-1 1:1000 (Cell Signaling, USA), rabbit phospho-SAPK/JNK (Thr 183/Tyr185) (p-JNK) 1:500 (Cell Signaling, USA) this antibody recognizes altogether the phosphorylated bands (46 and 54 kDa) of JNK1, JNK2 and JNK3; rabbit SAPK/JNK 1:1000 (Millipore, Italy).

2.6. Quantitative analysis of phosphorylated proteins

The band intensities were quantified using IMAGE J. All the quantification have been normalized for the β-actin levels in the same membrane. For the quantification of the phosphorylated proteins, the optical density (OD) of total and phophorylated protein bands were normalized to their respective β-actin controls on the same blot. The normalized phosphorylated proteins intensity was then measured over the normalized total protein intensity. The final calculations were performed according to the formula: [(OD phospho-protein/OD β-actin):(OD total protein/ OD β-actin)] and expressed as percentage of $Ddo^{+/+}$ 2 M.

2.7. Immunohistochemistry

$Ddo^{+/+}$ and $Ddo^{-/-}$ mice of 2 and 15 months of age ($n = 3$ per genotype and age) were deeply anesthetized and transcardially perfused with 4% (wt/vol) paraformaldehyde/0.1 M phosphate buffer, pH 7.4. Brains were cut into 10-μm-thick serial coronal sections, and sections from PFC and hippocampus were processed for immunoperoxidase by incubation with the primary mouse monoclonal PHF-1 tau-phosphorylated serine sites at 396 and 404 antibody (mA #56484, Bio-Rad Laboratories, dilution 1:1000) or mouse monoclonal phospho-PHF-tau pSer202/Thr205 antibody (AT8, MN1020, Thermo Scientific, dilution 1:200) or β-amyloid precursor protein (APP) antibody (ThermoFisher Scientific 51–2700, dilution 1:800), each revealed by a specific biotinylated secondary anti-IgGs (Vector Laboratories, Burlingame, CA) antibody, followed by incubation in the avidin-biotin complex (ABC Kit; Vectastain, Vector) and 3–3′ diaminobenzidine revelation (DAB Sigma Fast, Sigma-Aldrich, Louis, MO U.S.A.). Quantification of each immunosignal density was performed by analyzing the PHF1or AT8- or β-APP-positive cells in 3×10^3 μm^2 of PFC area selected from the rostral, medial, and caudal level of PFC, near the median line, to be representative of the entire region for each hemisphere ($n = 3$ pairs of sections per animal; $n \sim 200 \pm 50$ immunoreactive cells). Digital images were acquired under constant light illumination and magnification using a digital camera operating on gray levels (JCV FC 340FX, Leica). Quantification of PHF1, AT8, and β-APP peroxidase-based immunostaining was performed by measuring optical density using the image analysis software Image Pro Plus® 6.0 (MediaCybernetics) operating on a logarithmic scale of absorbance. In each section, the optical density zero value was assigned to the background (*i.e.*, a tissue portion devoid of stained cells).

2.8. ELISA assay

Brain regions were extracted at 100 μg/μl in extraction buffer (50 mM Tris-HCl pH 7.6, 0.01% NP-40, 150 mM NaCl, 2 mM EDTA, 0.1% SDS, 1 mM phenylmethylsulfonyl fluoride) containing protease inhibitor cocktail (Sigma) and then sonicated. The samples were centrifuged for 30 min at 4 °C at 10,000 × *g* and the supernatant was collected. Total protein concentration was then determined using a bicinchoninic acid protein assay kit according to the manufacturer's instructions (BCA protein assay, Thermo Scientific, Rockford, IL, USA).

The concentration of soluble Aβ40 and Aβ42 in the soluble protein fraction was determined by ELISA measurements using the mouse/rat amyloid β (1–40) and the mouse/rat amyloid β (1–42) assay kits (IBL International). All brain samples were diluted to within the detection limits of the test and analyzed in duplicate according to the manufacturer's instructions. Optical density (OD) values were measured at 450 nm using an ELISA plate reader (Labtech International Ltd., Heathfield, UK).

2.9. Human tissue samples collection

Human brain samples were obtained from The Netherlands Brain Bank (NBB), Netherlands Institute for Neuroscience, Amsterdam (open access: www.brainbank.nl). All material has been collected from donors for or from whom a written informed consent for a brain autopsy and the use of the material and clinical information for research purposes had been obtained by the NBB. Groups did not differ significantly for both age (Ctrl *vs* AD patients, mean ± SEM of years: 84.5 ± 1.4 *vs* 85.0 ± 0.8, $p = .98$, Mann Whitney test) and *postmortem* delay (Ctrl *vs* AD patients, mean ± SEM of hours: 5.8 ± 0.2 *vs* 5.6 ± 0.3, $p = .36$, Mann Whitney test). Details are reported in Table 1. The control subjects had no known clinical history of neurological or psychiatric disorders and were also fully neuropathologically evaluated to confirm that they were free of neurodegenerative pathologies. All patients had a clinical diagnosis of dementia or probable AD, according to National Institute of Neurological and Communicative Disorders and Stroke and the Alzheimer's Disease and Related Disorders Association (NINCDS-ADRDA) criteria (McKhann et al., 1984). Tissue blocks were dissected from superior frontal gyrus of each individual (Table 1), frozen rapidly, stored at 80 °C, and handled on dry ice to avoid thawing and RNA degradation.

2.10. High-performance liquid chromatography analysis

Brain tissue samples were analyzed as previously reported (Nuzzo et al., 2017). Samples were homogenized in 1:20 (w/v) 0.2 M TCA, sonicated (3 cycles, 10 s each) and centrifuged at 13,000 × *g* for 20 min. The precipitated protein pellets were stored at −80 °C for protein quantification, while the supernatants were neutralized with NaOH and subjected to precolumn derivatization with o-phthaldialdehyde/*N*-acetyl-L-cysteine. Diastereoisomer derivatives were resolved on a Simmetry C8 5-μm reversed-phase column (Waters, 4.6 × 250 mm).

Table 1
Demographic and clinical characteristics of Alzheimer's disease and non-demented control subjects.

Control					Alzheimer's disease				
ID	Sex	Age (years)	PMD (hours)	Clinical diagnosis	ID	Sex	Age (years)	PMD (hours)	Clinical diagnosis
1	M	79	5.45	Non-demented control	1	M	88	4.40	Alzheimer's disease
2	M	83	5.15	Non-demented control	2	M	87	6.10	Alzheimer's disease
3	M	83	5.45	Non-demented control	3	M	83	6.10	Alzheimer's disease
4	M	79	6.30	Non-demented control	4	M	82	5.15	Alzheimer's disease
5	M	90	5.45	Non-demented control	5	M	81	7.50	Alzheimer's disease
6	M	89	6.50	Non-demented control	6	M	88	5.30	Alzheimer's disease
7	M	88	7.00	Non-demented control	7	M	82	4.15	Alzheimer's disease
8	M	79	6.30	Non-demented control	8	M	85	7.10	Alzheimer's disease
9	M	87	6.05	Non-demented control	9	M	86	5.10	Alzheimer's disease
10	M	88	4.43	Non-demented control	10	M	88	5.10	Alzheimer's disease
Total	Total	Mean ± SEM	Mean ± SEM		Total	Total	Mean ± SEM	Mean ± SEM	
10	10	84.5 ± 1.4	5.8 ± 0.2		10	10	85.0 ± 0.8	5.6 ± 0.3	

M = male, AD = Alzheimer's Disease, PMD = *postmortem* delay.

Identification and quantification of D-Ser, L-Ser, D-Asp, and L-Asp were based on retention times and peak areas, compared with those associated with external standards. The identity of D-Asp, L-Asp, and D-Ser peaks was confirmed by adding known amount of external standards and by the selective degradation catalyzed by the RgDAAO M213R variant (Sacchi et al., 2002), StLASPO (Bifulco et al., 2013) and wild-type RgDAAO (Molla et al., 2000), respectively. Then, 10 μg of the enzymes were added to the samples, incubated at 30 °C for 60 min, and subsequently derivatized. Total protein content of homogenates was determined by using the Bradford assay method, after resolubilizing the TCA-precipitated protein pellets. The total concentration of amino acids detected in tissue homogenates was normalized by the total protein content and expressed as nmol/mg protein.

2.11. RNA extraction and quantitative real-time PCR analysis

Total RNA was extracted from tissues *postmortem* using miRNeasy® kit (Qiagen, Hilden, Germany) according to the manufacturer's instructions. RIN of samples was assessed using Biorad Experion Automated electrophoresis Station (Hercules, CA) prior to cDNA synthesis with Quantitect reverse transcription (Qiagen, Hilden, Germany). Total RNA (0.5 μg per sample) was used to synthesize cDNA. Quantitative Real-time PCR with Real Time ready catalog Assays (Roche Diagnostics) and LightCycler® 480 Probe Master (Roche Diagnostics) was performed on a Light Cycler 480 Real Time PCR system with 96-well format (Roche Diagnostics). All measurements from each subject were performed in duplicate. DDO mRNA expression levels were normalized to the mean of two housekeeping genes: β-actin and cyclophilin (PPIA). The following primers were used for cDNA amplification: DDO-fw 5′-GGTGTTCATTTGGTATCAGGTTG-3′ and DDO-rev 5′-CTTTCGAAATCCCAGAACCA-3′; β-actin-fw 5′-TCCTCCCT GGAGAAGAGCTA-3′ and β-actin-rev 5′-CGTGGATGCCACAGGACT-3′; PPIA-fw 5′-TTCATCTGCACTGCCAAGAC-3′ and PPIA-rev 5′-CACTTTG CCAAACACCACAT-3′. DDO mRNA expression was calculated using the relative quantification method ($2^{-\Delta\Delta Ct}$).

3. Results

3.1. D-aspartate induces NMDAR-dependent toxicity and triggers caspase-3 activation and JNK phosphorylation in primary cortical neurons

We have previously reported that persistent elevation of D-Asp levels in $Ddo^{-/-}$ brains is associated with caspase-3 activation, cell death, and the appearance of dystrophic microglia in cortical pyramidal neurons, likely *via* NMDAR (Cristino et al., 2015; Punzo et al., 2016). To ascertain the causal role of NMDAR activation in D-Asp-mediated cell death, we treated primary cortical neuronal cells with different concentrations of D-Asp, L-aspartate (L-Asp), and NMDA (ranging from 10 to 100 μM) at 12 days *in vitro* (DIV). Viability was examined 48 h after treatment by MTT assay (Esposito et al., 2012). Results showed that the increasing cell death is proportional to the D-Asp, L-Asp, and NMDA concentrations (one-way ANOVA, D-Asp: $F_{(3,33)} = 413.7$, $p < .0001$; L-Asp: $F_{(3,30)} = 197.50$, $p < .0001$; NMDA: $F_{(3,32)} = 203.70$, $p < .0001$; Fig. 1A). In particular, survival after D-Asp exposure was 84.79 ± 1.40% at 10 μM, 53.0 ± 3.5% at 50 μM (data not shown), and 29.70 ± 2.44% at 100 μM (Fig. 1A). By contrast, L-Asp and NMDA administration did not significantly affect survival at 10 μM (Fig. 1A), while they exerted a significant cytotoxic effect at 100 μM (Fig. 1A). The D-Asp-, L-Asp-, and NMDA-induced cell death effect was rescued by the noncompetitive NMDAR antagonist MK-801 (10 μM) (Fig. 1A). Moreover, in line with previous pharmacological studies (Errico et al., 2011a), the selective blockade of GluN2B-containing NMDARs by Ifenprodil (IFP, 10 μM) strongly attenuated D-Asp-dependent toxicity (81.26 ± 3.28% survival at 100 μM D-Asp; Fig. 1B). Finally, pretreatment with MTEP (5 μM), a selective inhibitor of metabotropic glutamate receptor mGlu5, partially decreased the cell death elicited by 100 μM D-Asp (41.95 ± 0.57% survival; Fig. 1B). Then, we investigated the kinetics of D-Asp-induced cell death in primary cortical neurons at both 10 and 100 μM (Fig. 1 c–d, g–h). MTT assay indicated that 100 μM D-Asp promoted a faster onset and more pronounced neuronal death than exposure to 10 μM (one-way ANOVA: 10 μM D-Asp, $F_{(6,43)} = 2.52$, $p = .03$; 100 μM D-Asp, $F_{(6,46)} = 22.14$, $p < .0001$; Figs. 1C, G). In particular, exposure to 100 μM D-Asp produced neuronal death already after 6 h (Fig. 1G), whereas a significant neurotoxic effect at the lower dose was only detected after 24 h (Fig. 1C). Furthermore, 48 h after administration, 10 μM D-Asp treatment induced cell death in ~20% of neurons (Fig. 1C), whereas 100 μM D-Asp induced ~55% neuronal loss (Fig. 1G). Notably, and consistently with NMDAR activation, the D-Asp-dependent neurotoxic effect was fully prevented by MK801 pretreatment (Fig. 1C, G). Then, we detected D-Asp-dependent release of *lactate dehydrogenase* (Van Veldhoven et al., 1991) in primary cortical neurons as a marker of lysed cells (Burd and Usategui-Gomez, 1973) (Fig. 1D, H). In agreement with the MTT assay, we observed that 100 μM D-Asp produced a significant LDH release 6 h after exposure (one-way ANOVA, $F_{(6,21)} = 84.39$, $p < .0001$; Fig. 1H), reaching its highest level at 48 h (Fig. 1H). Conversely, LDH release was slightly increased by 10 μM D-Asp only after 48 h (Fig. 1D). Remarkably, in line with NMDAR-dependent activation, MK801 completely prevented LDH leakage at both low and high D-Asp concentrations (Fig. 1D, H). Subsequently, we evaluated caspase-3 activation and activity in D-Asp-treated primary cortical neurons, as previously reported (Esposito et al., 2012) (Fig. 1E, F, I, J). Although Western blot analysis revealed that exposure to 10 μM D-Asp induced a significant degree of caspase-3 activation at 24 h (one-way ANOVA, $F_{(4,9)} = 11.73$,

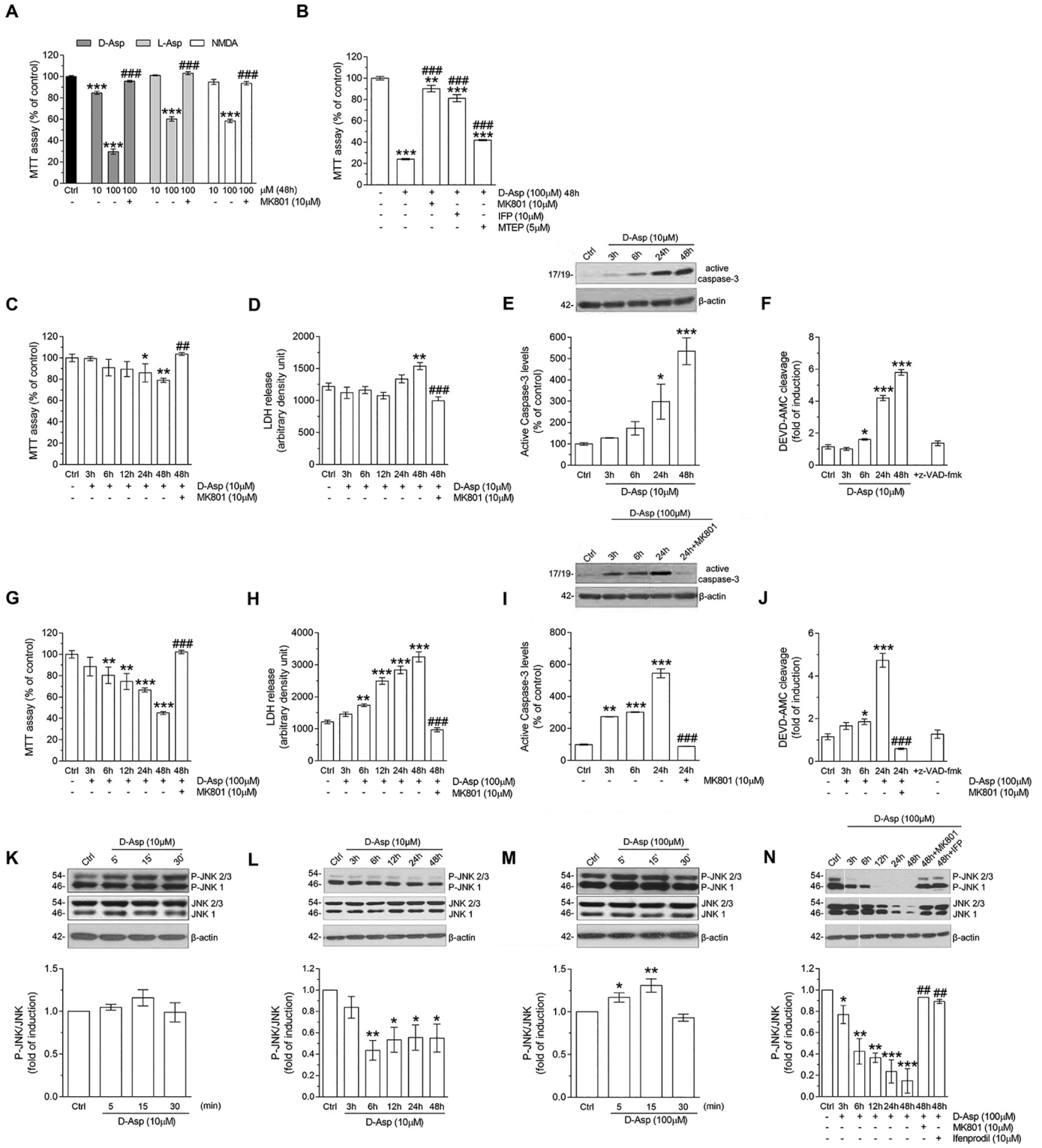

(caption on next page)

$p = .0013$; Fig. 1E), the activity of this enzyme, detected by DEVD-AMC cleavage, increased already at 6 h (one-way ANOVA, $F_{(5,19)} = 227.90$, $p < .0001$; Fig. 1F). At 100 µM, D-Asp prominently activated caspase-3 already after 3 h of exposure (one-way ANOVA, $F_{(4,7)} = 137.1$, $p < .0001$), achieving its maximum levels at 24 h (Fig. 1I). In addition, we found strong caspase-3 activity after 6 h, producing a peak at 24 h (Fig. 1J). Caspase-3 activation in cells treated with 100 µM D-Asp was fully prevented by MK801 (Figs. 1I, J). Finally, we tested whether D-Asp was also able to activate JNK in primary cortical neurons (Bessero et al., 2010; Borsello et al., 2003; Centeno et al., 2007). We found that D-Asp induced time-dependent changes in P-JNK levels (Fig. 1K, L, M, N). In detail, this D-amino acid elicited a rapid and transient increase in JNK phosphorylation at high, but not at low dose (one-way ANOVA; 10 µM: $F_{(3,24)} = 0.978$, $p = .42$; 100 µM: $F_{(3,20)} = 9.772$, $p = .0004$; Fig. 1K, M). JNK phosphorylation increased significantly already 5 min after exposure to 100 µM D-Asp, reached a peak at 15 min, and returned

Fig. 1. D-aspartate in primary cortical neurons induces NMDAR-dependent toxicity, and it is accompanied by increased caspase-3 activation and JNK phosphorylation. (A) DIV 12 cortical primary neurons were treated with D-aspartate (D-Asp), L-aspartate (L-Asp), and NMDA at the dose indicated. Survival was assessed 48 h later by MTT assay in the absence (−) and in the presence (+) of MK801 (10 μM) ($^{***}p < .0001$, *vs* Ctrl; $^{###}p < .0001$, compared to matched treatment). (B) DIV 12 cortical neurons were treated with 100 μM D-aspartate (D-Asp). Survival was assessed 48 h later by the MTT assay in the absence (−) and in the presence (+) of MK801 (10 μM), IFP (10 μM), and MTEP (5 μM) ($^{**}p < .01$; $^{***}p < .0001$, *vs* Ctrl; $^{###}p < .0001$, compared to 100 μM D-Asp). (C, G) Time course analysis of cell death induced by 10 (c) and 100 μM (g) of D-Asp in the absence (−) and in the presence (+) of MK801 measured by MTT assay ($^{*}p < .05$; $^{**}p < .01$; $^{***}p < .0001$, *vs* Ctrl; $^{##}p < .01$, $^{###}p < .0001$, compared to 48 h D-Asp treatment). (D, H) Time course analysis of cell death induced by 10 (d) e 100 μM (h) D-Asp in the absence (−) and in the presence (+) of MK801 detected by LDH assay ($^{**}p < .01$; $^{***}p < .0001$, *vs* Ctrl; $^{###}p < .0001$, compared to 48 h D-Asp treatment). Data from MTT and LDH analysis were expressed as mean ± SEM of % of Ctrl and arbitrary density unit, respectively. (E, I) Time course analysis of procaspase-3 activation detected by Western blotting analysis at 10 (e) and 100 (i) μM D-Asp. ($^{*}p < .05$,$^{**}p < .01$; $^{***}p < .0001$, *vs* Ctrl; $^{###}p < .0001$, compared to 24 h D-Asp treatment). Representative blots of 17-kDa caspase 3 fragment, detected by cleaved caspase-3 (Asp175) antibody by three independent experiments are shown in E (upper panel) and I (upper panel) after 10 and 100 μM of D-Asp administration, respectively. (F, J) Sisters cultures were lysed and assayed at time indicated for DEVD-AMC cleavage to detect caspase-3 activity after 10 (f) and 100 (j) μM D-Asp administration. Each data point represents the mean ± SEM of triplicate determinations of three independent experiments and is expressed as fold of induction of Ctrl (untreated cells) ($^{*}p < .05$, $^{***}p < .0001$, *vs* Ctrl; $^{###}p < .0001$, compared to 24 h D-Asp treatment). (K—N) Western blotting analysis of JNK phosphorylation (p-JNK) expression levels in lysates from Ctrl and D-Asp treated cells at 10 (K, L) and 100 μM (M, N). Quantification of p-JNK was normalized by total JNK immunoreactivity. Each data point represents the mean ± SEM of triplicate determinations of three independent experiments and is expressed as fold of induction of Ctrl (untreated cells) ($^{*}p < .05$, $^{**}p < .01$, $^{***}p < .0001$, *vs* Ctrl; $^{##}p < .01$, compared to 48 h D-Asp treatment). All experiments were analyzed by one-way ANOVA followed by Fisher *post hoc* comparison, when required.

to baseline levels at 30 min (Fig. 1M). Conversely, the persistent exposure to D-Asp at 10 and 100 μM for longer periods of time resulted in a progressive decline in JNK phosphorylation (one-way ANOVA; 10 μM: $F_{(15,19)} = 4.099$, $p = .01$, one-way ANOVA; 100 μM: $F_{(7,18)} = 12.53$, $p < .0001$, Figs. 1L, N). In particular, 10 μM D-Asp elicited a significant P-JNK reduction starting from 6 h after treatment (Fig. 1L), while 100 μM D-Asp was effective already 3 h after treatment (Fig. 1N). The effect of 100 μM D-Asp was fully prevented by MK801 and IFP pretreatment (Fig. 1N). In addition, 100 μM D-Asp also dramatically decreased the level of total JNK protein in cortical neurons (Fig. 1N, upper panel).

3.2. Lack of D-aspartate oxidase activity induces abnormal JNK phosphorylation and protein SUMOylation in the mouse prefrontal cortex

To extend the *in vitro* studies to an *in vivo* model, we evaluated the age-related effect of abnormally high D-Asp levels on JNK phosphorylation in the PFC of *Ddo*$^{-/-}$ mice. To this aim, cortical homogenates of *Ddo*$^{-/-}$ mice and their respective age-matched littermates were tested at the age of 2, 6, and 15 months (M). Western blot analysis revealed significantly increased JNK phosphorylation at 6 and 15 months compared to control brains (two-way ANOVA, age × genotype interaction, $F_{(2,12)} = 7.76$, $p = .007$), without any detectable variation in the level of total JNK protein (Fig. 2A).

The effect of *Ddo* gene deletion on brain aging was also examined by detecting the levels of other kinases involved in neuronal cell death and survival. Overall, we found a slight increase in the levels of phospho-AKT in young *Ddo*$^{-/-}$ mice compared to age-matched controls (two-way ANOVA, age × genotype interaction, $F_{(1,8)} = 14.51$, $p = .0052$; (Fig. 2B, I). Moreover, in the PFC of elderly mice we reported decreased phospho-AKT content in both genotypes (two-way ANOVA, age effect, $F_{(1,8)} = 104.4$, $p < .0001$), although this reduction was more pronounced in *Ddo*$^{-/-}$ mice (Fig. 2B, I). Conversely, total levels of AKT did not change between genotypes at the two ages analyzed (two-way ANOVA, age × genotype interaction, $F_{(1,8)} = 1.722$, $p = .22$; Fig. 2C, I). Moreover, despite a ~25% decrease in the total amount of GSK3ß in the PFC of old *Ddo*$^{-/-}$ mice compared to age-matched controls (two-way ANOVA, age × genotype interaction, $F_{(1,8)} = 4.83$, $p = .05$; Fig. 2E, I), no significant alterations in phospho-GSK3ß were observed either in young or old knockout mice (two-way ANOVA, age × genotype interaction, $F_{(1,8)} = 4.89$, $p = .06$; Fig. 2D, I). Interestingly, a slight increase in phospho-ERK1/2 was detected in the PFC of 2 M-old *Ddo*$^{-/-}$ mice (two-way ANOVA, age × genotype interaction, $F_{(1,8)} = 8.34$, $p = .02$ Fig. 2F, I), while no significant changes were observed in aged mice (Figs. 2F, I). In addition, we found comparable levels of total ERK1/2 between genotypes at both ages analyzed (two-way ANOVA, age × genotype interaction, $F_{(1,8)} = 2.00$, $p = .19$; Fig. 2G, I). Finally, the levels of p35, the neuronal-specific activator of Cdk5, were unaltered in the PFC of both genotypes (two-way ANOVA, age × genotype interaction, $F_{(1,8)} = 2.06$, $p = .19$; Fig. 2H, I).

Next, we investigated protein SUMOylation levels, known to be associated with oxidative stress in cell cultures (Feligioni et al., 2011; Stankovic-Valentin et al., 2016) and in animal models of AD (Marcelli et al., 2017) and connected with JNK activation (Feligioni et al., 2011). Interestingly, Western blot experiments revealed an overall increase in SUMO1 protein levels in the PFC of *Ddo*$^{-/-}$ mice at all ages analyzed compared to *Ddo*$^{+/+}$ littermates (two-way ANOVA, age × genotype interaction, $F_{(2,12)} = 9.22$, $p = .004$; Fig. 2J).

3.3. Lack of D-aspartate oxidase activity is associated with age-related changes in Tau phosphorylation in the mouse prefrontal cortex

Based on the knowledge that JNK proteins modulate *in vitro* Tau phosphorylation at many serine/threonine-proline AD-specific sites (Augustinack et al., 2002; Yoshida et al., 2004) and that abnormally high levels of D-Asp affect JNK phosphorylation in cortical primary neurons and in *Ddo*$^{-/-}$ brains, we investigated the state of Tau phosphorylation in the PFC of these mutants at 2 and 15 months of age by Western blotting. Statistical analysis showed that total Tau protein expression in 2 M- and 15 M-old *Ddo*$^{-/-}$ mice was comparable to *Ddo*$^{+/+}$ littermates (two-way ANOVA, age × genotype interaction, $F_{(1,8)} = 0.85$ $p = .38$; Fig. 3A, H). Similarly, we failed to find significant differences in Tau-1, Tau phosphorylation at the Ser396 and Thr231 sites in young and old *Ddo*$^{-/-}$ mice, compared to their age-matched controls (two-way ANOVA, Tau1: age × genotype interaction, $F_{(1,8)} = 0.18$, $p = .68$; Ser396: age × genotype interaction, $F_{(1,8)} = 1.21$, $p = .30$; Thr231: age × genotype interaction, $F_{(1,8)} = 0.27$, $p = .62$; Fig. 3B, D,G, H). Conversely, in the same brain samples, we found a significant age × genotype interaction on Tau phosphorylation levels at the PHF1 and AT8 sites (two-way ANOVA; PHF1: age × genotype interaction, $F_{(1,8)} = 14.13$, $p = .005$; AT8: age × genotype interaction, $F_{(1,8)} = 11.43$, $p = .009$; Fig. 3E, F, H). Interestingly, *post-hoc* comparisons showed Tau protein hypophosphorylation in old *Ddo*$^{-/-}$ mice at the PHF1 and AT8 sites compared to the age-matched control mice (around 50% and 45% decrease, respectively) (Fig. 3E, F, H). Furthermore, we also found a considerable tendency for AT270 Tau phosphorylation to decrease in 15 M-old *Ddo*$^{-/-}$ mice compared to controls (two-way ANOVA; age × genotype interaction, $F_{(1,8)} = 2.67$, $p = .14$; Fig. 3C, H).

Next, we performed immunohistochemical analysis of AT8 and PHF1 on PFC slices of *Ddo*$^{-/-}$ mice at 2 and 15 months of age. In line with Western blotting data, we detected a trend for AT8-positive cells to decrease in old *Ddo*$^{-/-}$ mice compared to controls (two-way ANOVA; age × genotype interaction, $F_{(1,8)} = 0.15$, $p = .70$; Fig. 3I–L, Q).

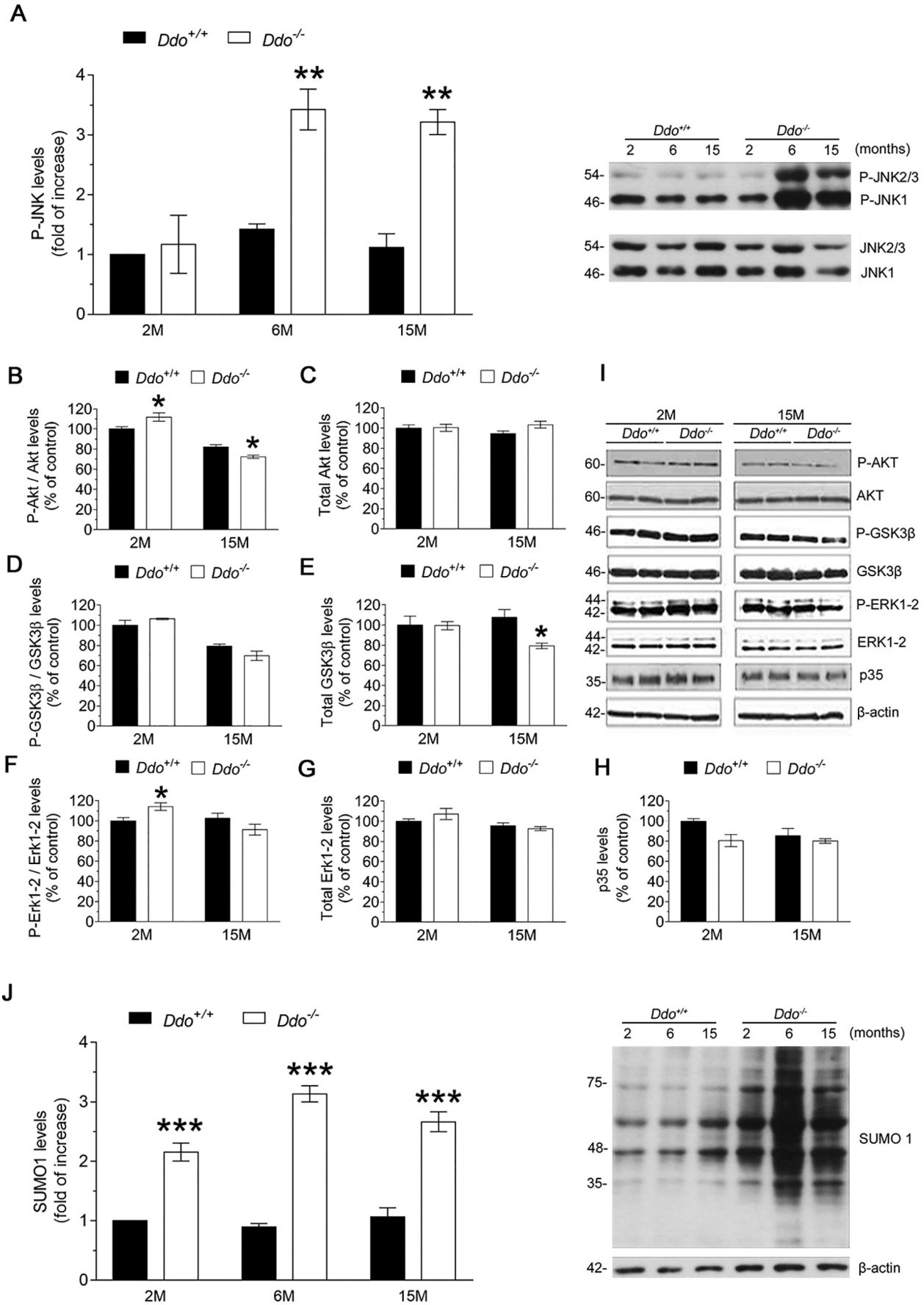

(caption on next page)

Fig. 2. Lack of D-aspartate oxidase activity induces abnormal cortical levels of JNK phosphorylation and SUMOylation. (A) Representative Western blot and quantification of JNK phosphorylation (P-JNK) expression levels in cortical lysates from *Ddo*$^{+/+}$ and *Ddo*$^{-/-}$ mice at different months of age. Quantification of P-JNK was calculated as ratio between P-JNK and total JNK immunoreactivity by running the experiments in triplicate. Results are expressed as means ± SEM of fold of increase *vs.* P-JNK levels of controls (*Ddo*$^{+/+}$ 2 M). (**$p < .01$ compared with the age-matched *Ddo*$^{+/+}$). (B–H) Quantification of immunoreactivity of P-Akt (B), total Akt (C), P-GSK3β (D), total GSK3β (E), P-ERK1/2 (F), total ERK1/2 (G), and p35(H) kinases levels in the PFC of *Ddo*$^{-/-}$ mice compared to *Ddo*$^{+/+}$ littermates at 2 M and 15 M. Values of phosphorylated proteins were normalized by total protein levels; total protein values were normalized by β-actin levels. All values are expressed as means ± SEM of percentage of Ctrl (*Ddo*$^{+/+}$ 2 M). (*$p < .05$ compared with age-matched *Ddo*$^{+/+}$). (I) Representative Western blot of cortical lysates of *Ddo*$^{-/-}$ mice at 2 and 15 months of phospho-AKT (p-AKT), total AKT, phospho–Ser9-GSK3β (inactive form) (p-GSK3β), total GSK3β (active), p35 (the neuronal-specific activator of Cdk5, phospho-Thr202,Tyr204-ERK1/2 (p-ERK1/2), and total ERK1/2. All densitometry values are corrected by β-actin levels and expressed as percentage of Ctrl (*Ddo*$^{+/+}$ 2 M). (J) Representative Western blot and quantification of SUMO-1 expression levels in cortical lysates of *Ddo*$^{+/+}$ and *Ddo*$^{-/-}$ mice at different months of age. SUMO-1 immunoreactivity was detected by using a specific antibody and normalized by β-actin levels. Quantification of SUMO-1 expression levels was calculated by running the experiments in triplicate. Results are expressed as means ± S.E.M of the fold of increase *vs.* the SUMO-1 levels of Ctrl (*Ddo*$^{+/+}$ 2 M). (***$p < .001$, *vs.* age-matched *Ddo*$^{+/+}$). All experiments were analyzed by two-way ANOVA followed by Fisher *post hoc* comparison, when required.

Furthermore, we found significant age-related changes in PHF1 immunodensity in *Ddo*$^{-/-}$ mice compared to *Ddo*$^{+/+}$ littermates (two-way ANOVA; age × genotype interaction, $F_{(1,8)} = 44.83$, $p = .0002$; Fig. 3M–P, R). In agreement with Western blotting, *post-hoc* analysis showed decreased levels of PHF1-positive cells immunodensity in the PFC of 15 M-old *Ddo*$^{-/-}$ mice compared to their age-matched controls (Fig. 3M–P, R).

3.4. D-aspartate induces Tau hypophosphorylation and cleavage in cortical primary neurons

To investigate the direct association between D-Asp exposure, NMDAR activation, and Tau phosphorylation, we treated primary cortical neurons with 10 or 100 μM D-Asp in the presence or absence of MK801 (10 μM). Interestingly, we found that administration of 10 μM D-Asp induced a significant time-dependent decrease in Tau phosphorylation at PHF1 (one-way ANOVA; $F_{(5,12)} = 6.81$, $p = .0031$, Fig. 4B, E) and AT270 sites (one-way ANOVA; $F_{(5,12)} = 4.33$, $p = .02$, Fig. 4C, E). Conversely, no changes were detected in total Tau protein and Tau-1 immunodensity (one-way ANOVA; total Tau: $F_{(5,12)} = 0.64$, $p = .67$; Tau-1: $F_{(5,12)} = 0.69$, $p = .64$; Fig. 4A, D, E). Differing from the lower dose, 100 μM D-Asp induced an early and robust decrease in the amount of total Tau protein (one-way ANOVA; $F_{(5,12)} = 11.99$, $p = .0003$; Fig. 4F, J) and the appearance of a ~17 kDa Tau fragment from 6 h of D-Asp exposure (Fig. 4J upper panel). This fragment, which accumulates over time, resembles the N-terminal, toxic fragment of Tau, previously reported to be produced during neuronal death (Amadoro et al., 2006; Amadoro et al., 2004; Canu et al., 1998). In line with the decrease in total Tau levels, we also found a similar time-dependent reduction in the phosphorylation of PHF1 (one-way ANOVA; $F_{(5,15)} = 81.80$, $p < .0001$; Fig. 4G, J) and AT270 sites (one-way ANOVA, $F_{(5,12)} = 78.59$, $p < .0001$; Fig. 4H, J). In contrast, exposure to 100 μM D-Asp was associated with opposite, time-dependent fluctuations in Tau-1 levels since this dephosphorylated site was substantially upregulated from 3 to 24 h after administration, before decreasing at 48 h, as compared to untreated primary cortical neurons (one-way ANOVA; $F_{(5,12)} = 48.18$; Figs. 4I, J). Finally, we showed that MK-801 pretreatment prevented the D-Asp-dependent modifications in Tau protein at both doses tested (Fig. 4B, C, E, F–J), thus indicating a direct role of NMDAR activation in the molecular effects exerted by D-Asp upon tau metabolism.

3.5. Lack of D-aspartate oxidase activity does not affect cortical production of β-amyloid 1–40 and 1–42 peptides in mice

Several lines of evidence show that JNK activation affects the metabolism of β-amyloid precursor protein (β-APP), leading to Aß42-mediated cell death (Colombo et al., 2009; Tare et al., 2011). Based on these findings, we measured β-APP protein levels in the mouse PFC in order to assess whether the increase in cortical JNK phosphorylation influences β-APP metabolism in aged *Ddo*$^{-/-}$ mice. Western blotting analysis did not reveal any significant changes in β-APP protein expression in the PFC of 2 M- and 15 M-old *Ddo*$^{-/-}$ mice compared to the age-matched controls (two-way ANOVA, age × genotype interaction, $F_{(1,8)} = 0.31$, $p = .60$; Fig. 5A). However, quantification of β-APP immunohistochemistry performed with anti-C-terminal APP antibody (Fig. 5B–F) demonstrated a significant age × genotype interaction in this brain region (two-way ANOVA, age × genotype interaction, $F_{(1,8)} = 13.05$, $p = .007$; Fig. 5F). Interestingly, *post-hoc* comparison revealed an approx. 2-fold increase in β-APP immunodensity in 15 M *Ddo*$^{-/-}$ mice compared to their age-matched controls (Fig. 5F). Notably, in both genotypes at 15 months of age, APP-positive cells appeared rounded and shrunk compared to APP-positive cells in young littermates, as shown in the images at high magnification. This finding, which likely reflects physiological age-related neuronal shrinkage and decline in axonal transport (Milde et al., 2015), appeared to be more pronounced in the PFC of *Ddo*$^{-/-}$ mice than in their *Ddo*$^{+/+}$ littermates (Fig. 5F). Based on the recent findings suggesting a role for D-Asp in the biochemical processes that lead to the formation of Aβ40 and Aβ42 aggregates (D'Aniello et al., 2017), we also evaluated the amount of such ß-amyloid peptides in the PFC homogenates of *Ddo*$^{+/+}$ and *Ddo*$^{-/-}$ mice by using a highly sensitive rodent-specific ELISA assay. Statistical analysis revealed unaltered Aβ40 and Aβ42 levels in *Ddo*$^{-/-}$ mice compared to *Ddo*$^{+/+}$ animals at both 2 and 15 months of age (two-way ANOVA; Aβ40: age × genotype interaction $F_{(1,14)} = 0.83$, $p = .38$; Aβ42: age × genotype interaction $F_{(1,15)} = 0.11$, $p = .73$; Fig. 5G, H).

3.6. Analysis of Tau phosphorylation and β-APP metabolism in the hippocampus of *Ddo*$^{-/-}$ mice

We analyzed the age-dependent changes in Tau phosphorylation and β-APP metabolism also in another AD-relevant brain area, like the hippocampus.

First, we assessed by immunohistochemical analysis the distribution and the amount of phosphorylated Tau at AT8 and PHF1 sites in the CA3 and dentate gyrus (DG) of 2 M- and 15 M-old *Ddo*$^{-/-}$ mice. Differently to what observed in the PFC, statistical analysis revealed a significant age × genotype interaction on AT8 immunodensity in both CA3 and DG hippocampal regions (two-way ANOVA, age × genotype interaction, CA3: $F_{(1,8)} = 62.22$, $p < .0001$; DG: $F_{(1,8)} = 159.50$, $p < .0001$; Fig. 6A–F). The following *post hoc* comparisons showed increased AT8 immunoreactivity in the CA3 area of 2 M-old *Ddo*$^{-/-}$ mice compared to the aged-matched *Ddo*$^{+/+}$ littermates (Fig. 6A, B, E). On the other hand, we found unaltered AT8 positive cells number in 15 M-old *Ddo*$^{-/-}$ mice compared to controls (Fig. 6C–E). Furthermore, in the DG area, statistical analysis revealed an increase in AT8 immunodensity in 2 M-old *Ddo*$^{-/-}$ mice (Fig. 6A, B, F) along with a reduction in 15 M-old *Ddo*$^{-/-}$ mice, compared to their respective age-matched controls (Fig. 6C, D, F). Next, we evaluated PHF1 immunoreactivity on the same hippocampal sections. Similarly to AT8 analysis, two-way ANOVA evidenced a significant age × genotype interaction in both CA3 and DG (two-way ANOVA, age × genotype interaction, CA3: $F_{(1,8)} = 21.52$, $p = .0017$; DG: $F_{(1,8)} = 54.43$,

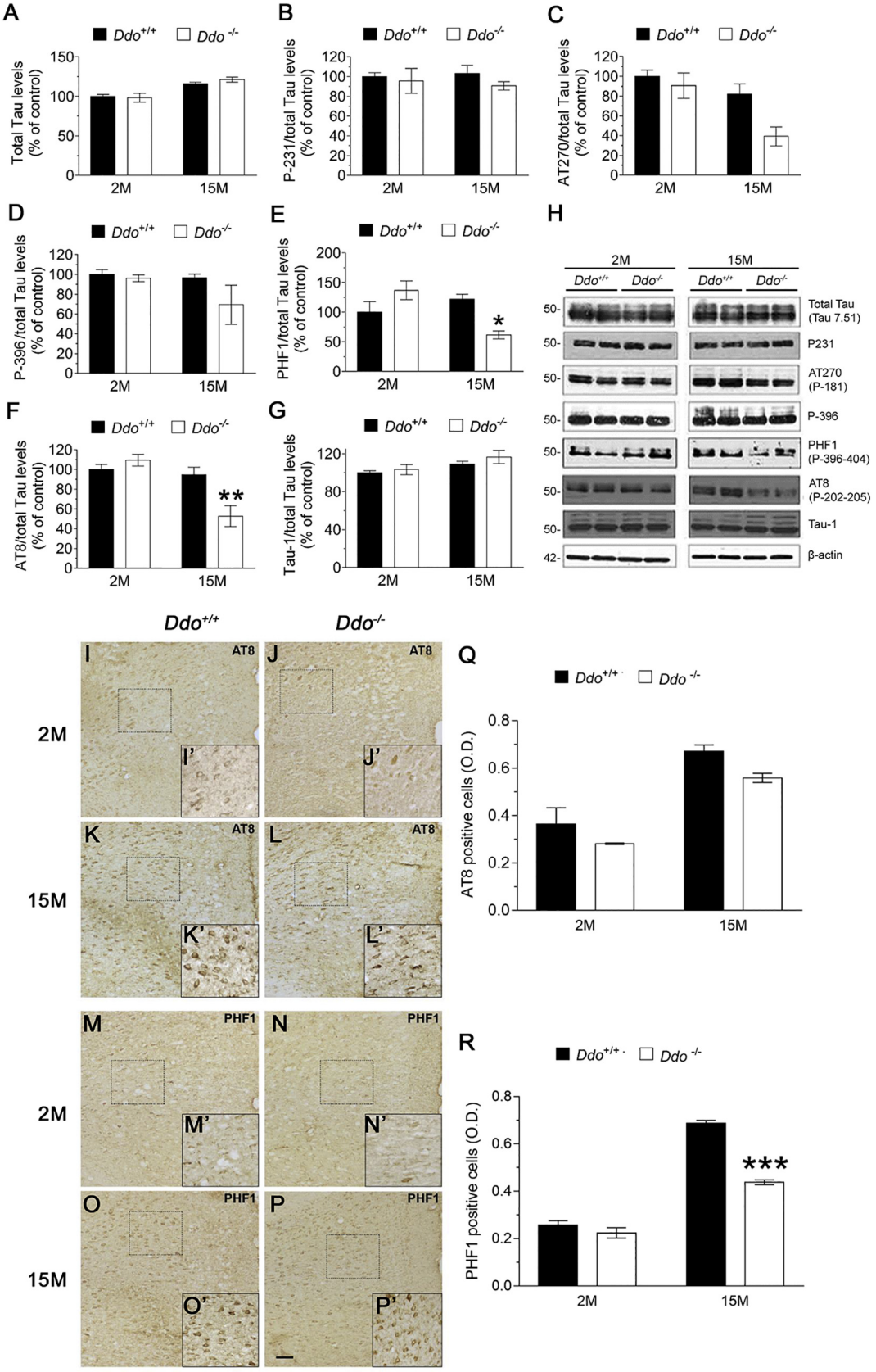

(caption on next page)

$p < .0001$; Fig. 6G–L). Specifically, in the CA3 area, PHF1 positive cells were increased in 2 M-old *Ddo*$^{-/-}$ mice while they were reduced in 15 M-old knockout animals, compared to their respective age-matched wild-type littermates (Fig. 6G–K). Conversely, in the DG, we found unaltered PHF1 positive cells between genotypes at 2 M of age while a significant PHF1 immunodensity reduction was observed in

Fig. 3. Lack of D-aspartate oxidase activity in mice is associated with age-related changes of Tau phosphorylation in cortex. (A–G) Quantification of protein levels of total Tau (A) and Thr231(B), AT270 (C), Ser 396 (D), PHF1 (E), AT8 (F), Tau-1 (G) Tau phosphorylated sites in the PFC of old and young *Ddo*$^{-/-}$ mice, compared to controls. All values are expressed as means ± SEM of % of Ctrl (*Ddo*$^{+/+}$ 2 M). ($^{*}p < .05$, $^{**}p < .01$ compared with age-matched *Ddo*$^{+/+}$). (H) Representative Western blot of cortical lysates of *Ddo*$^{-/-}$ mice at 2 and 15 months obtained by phosphorylation-dependent and site-specific tau antibodies (I–L, M–P). Representative immunostaining of Tau phosphorylation at the AT8 (I–L) and PHF1(M–P) sites in cortical slices of 2 M- and 15 M-old in *Ddo*$^{-/-}$ and *Ddo*$^{+/+}$ mice detected by immunohistochemical analysis. (I′– L', M'–P′) High magnification of (I′–L') AT8 and (M'–P′) PHF1 positive cells in the PFC region of 2 M- and 15 M-old *Ddo*$^{-/-}$ and *Ddo*$^{+/+}$ littermates. (Q, R) Bar graphs showing the optical density (O.D.) of (Q) AT8- and (R) PHF1-positive cells in cortical slices of 2 M- and 15 M-old in *Ddo*$^{-/-}$ and *Ddo*$^{+/+}$ mice. ($^{***}p < .0001$ compared with age-matched *Ddo*$^{+/+}$). Data are expressed as mean ± SEM. All experiments were analyzed by two-way ANOVA followed by Fisher *post hoc* comparison, when required.

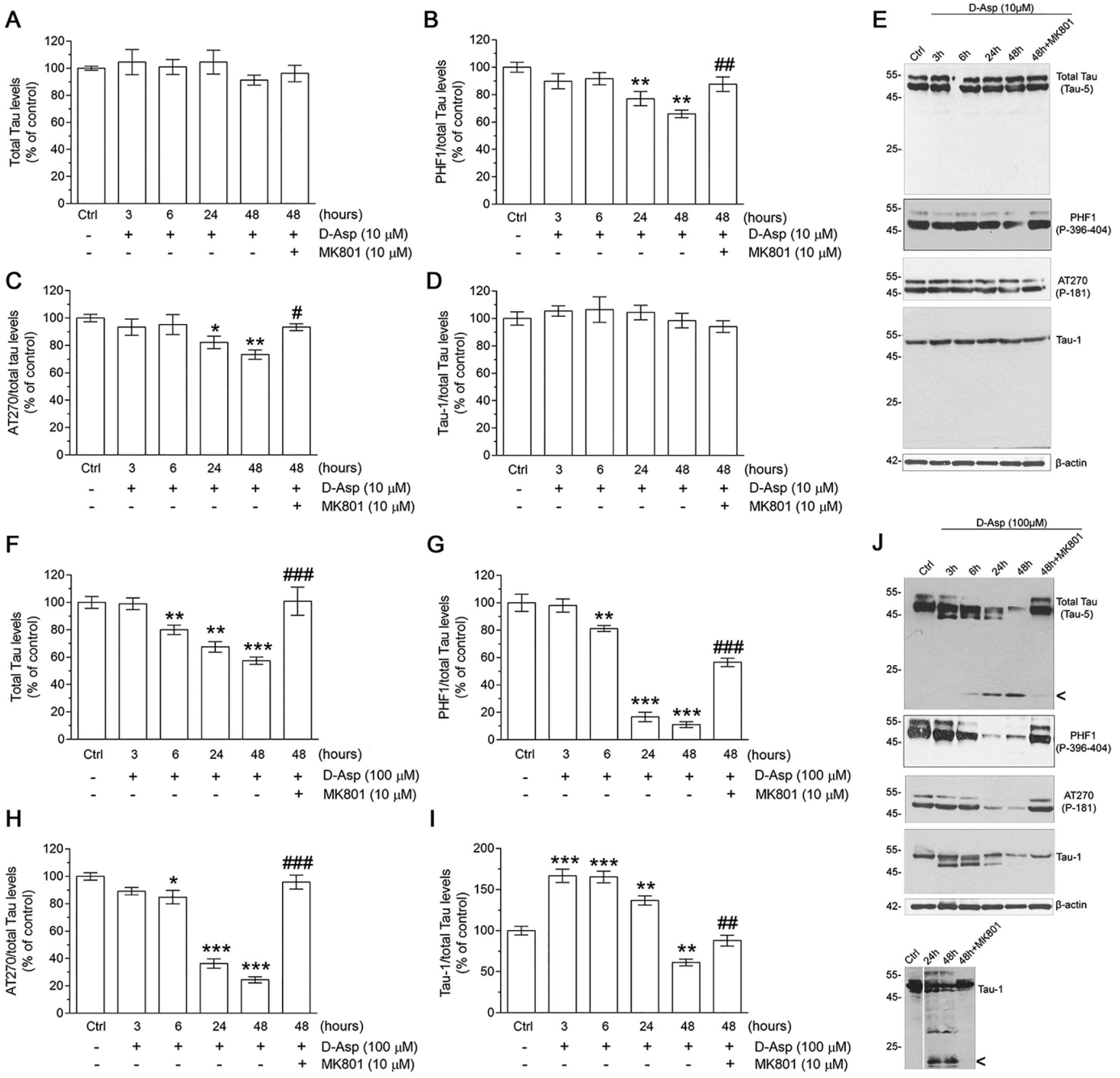

Fig. 4. Effect of D-Asp treatment on Tau protein phosphorylation in cortical primary neurons. DIV 12 cortical neurons were treated with D-Asp at the dose indicated in the absence (−) and in the presence (+) of MK801 (10 μM). (A, F) Time course analysis of total Tau protein expression detected by Tau-5 antibody induced by 10 (A) and 100 μM (F) of D-Asp in the absence (−) and in the presence (+) of MK801 (10 μM). (B–D) Time course analysis of Tau phosphorylation at the PHF1 (B) AT270 (C) and Tau-1 (D) sites induced by 10 μM D-Asp in the absence (−) and in the presence (+) of MK801 (10 μM). (G-I) Time course analysis of Tau phosphorylation at the PHF1 (G), AT270 (H) and Tau-1 (I) sites induced by 100 μM D-Asp in the absence (−) and in the presence (+) of MK801 (10 μM). (E, J) Analysis of Tau phosphorylation sites were assessed 48 h later by Western blotting analysis, as indicated by representative panels. All values are expressed as means ± SEM of % of Ctrl ($^{*}p < .05$, $^{**}p < .01$, $^{***}p < .0001$, compared to Ctrl; $^{\#}p < .05$, $^{\#\#}p < .01$, $^{\#\#\#}p < .0001$, compared to 48 h D-Asp). All values are expressed as mean ± SEM. All experiments were analyzed by one-way ANOVA followed by Fisher *post hoc* comparison, when required.

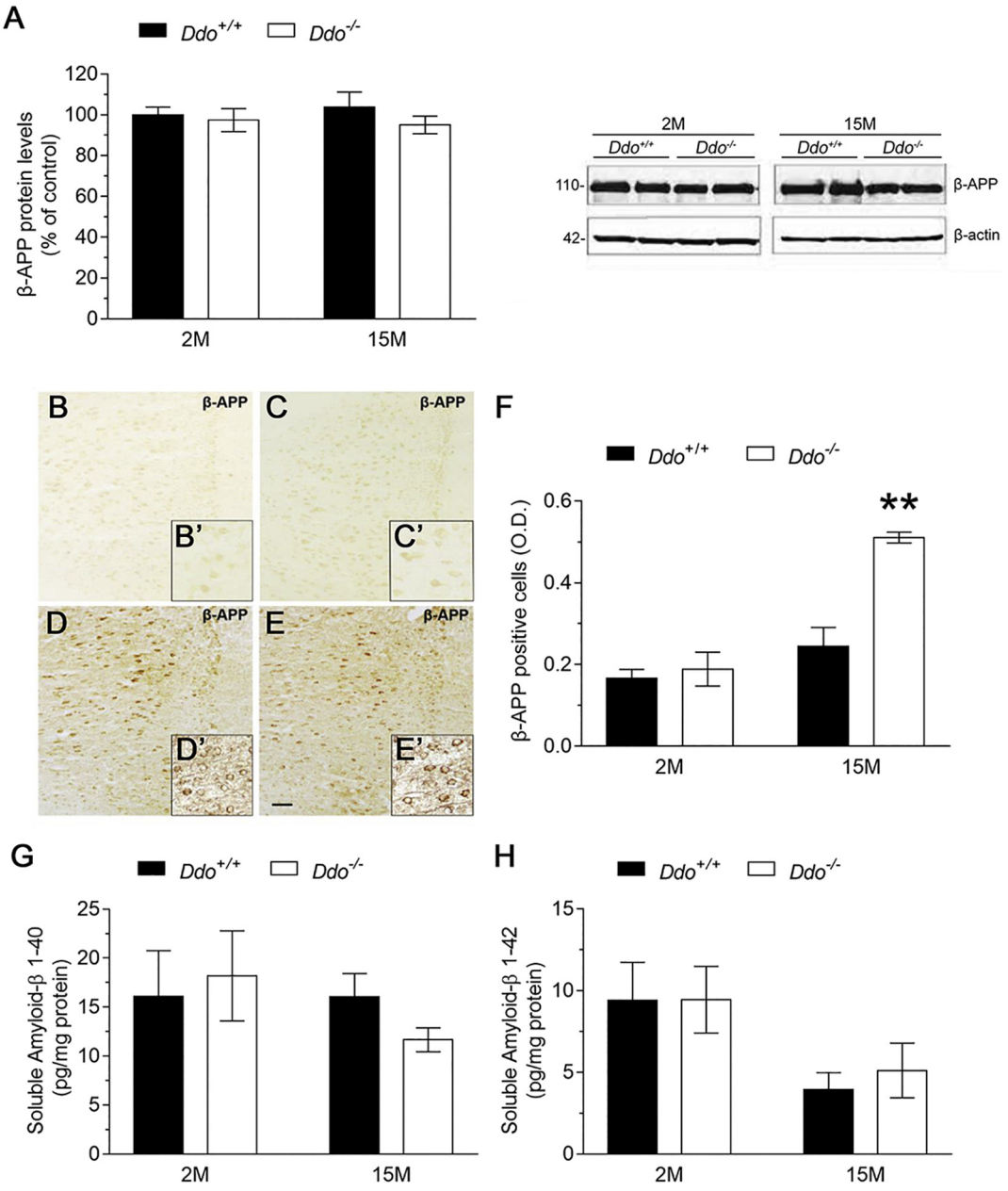

Fig. 5. Lack of D-aspartate oxidase activity does not affect β-Amyloid 1–40 and 1–42 peptides production. (A) Western blot analysis of full length β amyloid precursor protein (β-APP) levels in the PFC of *Ddo*$^{+/+}$ and *Ddo*$^{-/-}$ mice, at the two ages illustrated, detected by rabbit anti-C-terminal APP antibody. (B–E) APP immunostaining signal detected in the PFC of 2 M- and 15 M-old *Ddo*$^{-/-}$ mice, compared to the age-matched *Ddo*$^{+/+}$. (B′–E') High magnification of β-APP positive cells in the PFC region of 2 M- and 15 M-old *Ddo*$^{-/-}$ and *Ddo*$^{+/+}$ littermates. (F) Bar graphs showing the optical density (O.D.) of βAPP-positive cells in the PFC of 2 M- and 15 M-old in *Ddo*$^{-/-}$ and *Ddo*$^{+/+}$ mice. (**$p < .01$, compared to 15 M-old *Ddo*$^{+/+}$). All immunostaining signals from immunohistochemistry experiments are expressed as means ± SEM of O.D. (G, H) Analysis of endogenous Amyloidβ 1–40 (G) and 1–42 (H) peptides levels in PFC homogenates of *Ddo*$^{+/+}$ and *Ddo*$^{-/-}$ mice at 2 M and 15 M of age, detected by ELISA analysis. Values of ELISA experiments are expressed as mean ± SEM of pg/mg protein. All experiments were analyzed by two-way ANOVA followed by Fisher *post hoc* comparison, when required.

15 M-old *Ddo*$^{-/-}$ mice, compared to age-matched controls (Fig. 6G–J, L).

Then, we measured β-APP protein levels in the hippocampus of 2 M- and 15 M-old *Ddo*$^{-/-}$ mice by immunohistochemical and western blotting approaches. β-APP immunohistochemistry performed with anti-C-terminal APP antibody (Fig. 6M–P) indicated a non-significant age × genotype interaction in both CA3 and DG areas (two-way ANOVA, age × genotype interaction, $F_{(1,8)} = 0.02$, $p = .88$; Fig. 6M–R). Accordingly, western blotting analysis did not reveal significant changes in the expression levels of β-APP protein in the hippocampus of both 2 M- and 15 M-old *Ddo*$^{-/-}$ mice, compared to the age-matched controls (two-way ANOVA, age × genotype interaction, $F_{(1,8)} = 1.30$, $p = .29$; Fig. 6S). Finally, we evaluated the amount of β-amyloid peptides (Aβ40 and Aβ42) in the hippocampal homogenates of *Ddo*$^{+/+}$ and *Ddo*$^{-/-}$ mice by using a highly sensitive rodent-specific ELISA assay. Statistical analysis revealed unaltered Aβ40 and Aβ42 levels in *Ddo*$^{-/-}$ mice, compared to *Ddo*$^{+/+}$ mice, at both ages analyzed (two-way ANOVA, age × genotype interaction, Aβ40: $F_{(1,15)} = 0.70$, $p = .42$; Aβ42: $F_{(1,17)} = 3.46$, $p = .08$; Fig. 6T, U).

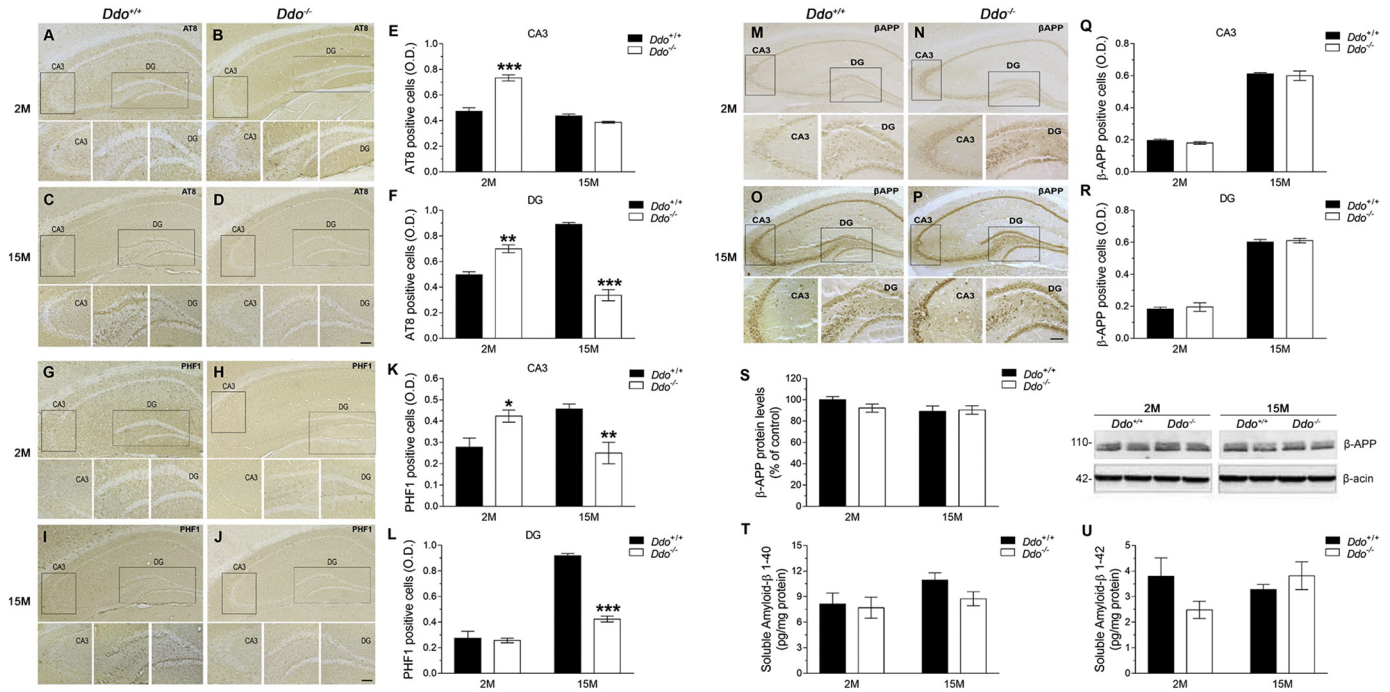

Fig. 6. Analysis of Tau phosphorylation, β-APP expression levels and β-Amyloid 1–40 and 1–42 peptides production in the hippocampus of *Ddo*$^{-/-}$ mice. (A–D, G–J, M–P) Representative immunostaining of Tau phosphorylation at the (A–D) AT8 and (G–J) PHF1 sites, and of (M–P) β-APP in the hippocampal slices of (A, B, G, H, M, N) 2 M- and (C, D, I, J, O, P) 15 M-old *Ddo*$^{-/-}$ and *Ddo*$^{+/+}$ mice. For each representative immunostaining, high magnifications panels are shown in the insets. (E, F, K, L, Q, R) Bar graphs showing the optical density (O.D.) of (E, F) AT8-, (K, L) PHF1- and (Q, R) β-APP-positive cells in the (E, K, Q) CA3 and (F, L, R) dentate gyrus (DG) area of 2 M- and 15 M-old *Ddo*$^{-/-}$ and *Ddo*$^{+/+}$ mice. All immunostaining signals from immunohistochemistry experiments are expressed as means ± SEM of O.D. (S) Western blot analysis of full length β-amyloid precursor protein (β-APP) levels in the hippocampal homogenates of *Ddo*$^{+/+}$ and *Ddo*$^{-/-}$ mice, at the two ages illustrated, detected by rabbit anti-C-terminal APP antibody. Representative blots comparing the two genotypes at the two ages reported are also shown. (T, U) Analysis of endogenous Amyloid β (T) 1–40 and (U) 1–42 peptides levels (expressed as mean ± SEM of pg/mg protein) in hippocampal homogenates of *Ddo*$^{+/+}$ and *Ddo*$^{-/-}$ mice at 2 M and 15 M of age, detected by ELISA. All experiments were analyzed by two-way ANOVA, followed by Fisher's *post hoc* comparison, when required ($^{*}p < .05$; $^{**}p < .01$; $^{***}p < .0001$, compared with age-matched *Ddo*$^{+/+}$).

3.7. Free D-aspartate levels and D-aspartate oxidase expression are unaltered in the superior frontal gyrus of patients with Alzheimer's disease

To translate *in vitro* and *ex vivo* studies to humans, we measured the endogenous levels of D-Asp and its L-enantiomer, L-Asp, in the superior frontal gyrus (SFG) of both patients affected by AD and nondemented subjects *postmortem* (obtained by Netherlands Brain Bank, Amsterdam, NL; $n = 10$/clinical condition) by using HPLC analysis. Statistical analysis showed comparable D-Asp levels between AD patients and controls (Mann-Whitney test, $p = .93$; Fig. 7A). Similarly, we did not observe any significant difference in the content of L-Asp between the two clinical conditions (Mann-Whitney test, $p = .39$; Fig. 7B). Consequently, the D-Asp/total Asp ratio was unchanged between groups (Mann-Whitney test, $p = .49$; Fig. 7C). Finally, we also analyzed *DDO* mRNA transcript levels in the same cohort of *postmortem* samples. According to neurochemical analysis, we found comparable *DDO* gene expression between AD patients and nondemented individuals (Mann-Whitney test; $p = .35$; Fig. 7D).

4. Discussion

Despite accumulating evidence pointed out a primary protective

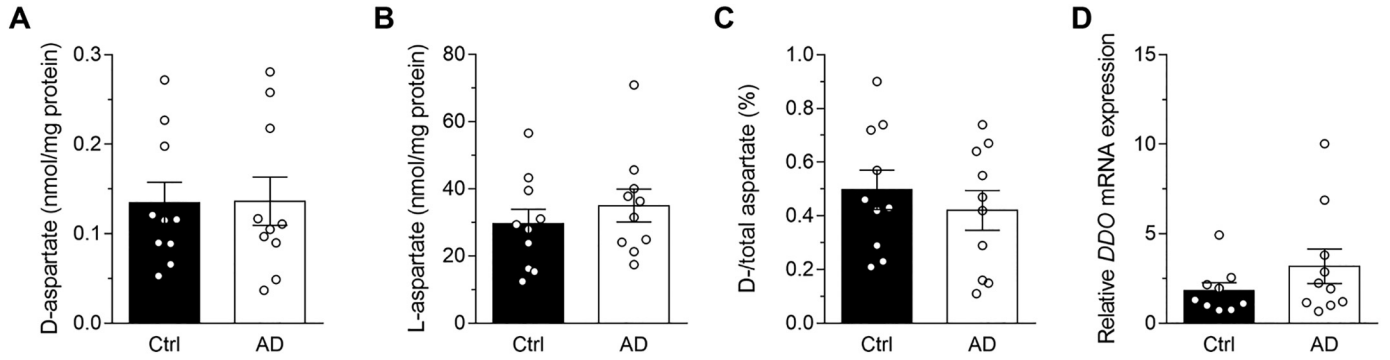

Fig. 7. Free D-Asp levels and *Ddo* mRNA expression in the postmortem superior frontal gyrus of patients affected by Alzheimer's disease. (A–C) Content of D-Asp (A), L-Asp (B) and D−/total Asp ratio (C) analyzed in the superior frontal gyrus of Alzheimer's disease patients (AD, $n = 10$) and healthy subjects (Ctrl, $n = 10$) detected by HPLC analysis. In each sample, all the analytes were detected in a single run by HPLC and expressed as nmol/mg protein. (D) Quantitative RT-PCR of *DDO* transcript in the *post mortem* superior frontal gyrus of patients affected by Alzheimer's disease (AD) and control individuals. All experiments were analyzed by Mann-Whitney test.

role of DDO activity against precocious age-dependent brain deterioration (Cristino et al., 2015; Errico et al., 2011b; Punzo et al., 2016), no mechanistic observations support the existence of a direct link between abnormally high D-Asp levels, NMDAR-related signaling, and neuronal demise.

In the present work, we showed that D-Asp exposure induces NMDAR-dependent cell death and caspase-3 activation, along with modulation of JNK and Tau phosphorylation levels in primary cortical neurons. Previous studies have identified JNK as a key element responsible for regulating NMDAR-related signaling, oxidative stress, and apoptosis, and its critical involvement for pathological cell death processes associated with neurodegenerative diseases (Jong et al., 2009; Nistico et al., 2015; Thomas et al., 2008). Here, in agreement with its pharmacological features, we report that administration of D-Asp to primary cortical neurons induces a biphasic modulation of JNK phosphorylation through NMDAR stimulation in a time- and dose-dependent manner. Therefore, consistent with the "double-edged sword" role of JNK activation in cell death (Liu and Lin, 2005), we argued that either the early JNK hyperphosphorylation or the subsequent, progressive JNK hypophosphorylation induced by D-Asp exposure are involved in neuronal death. However, further molecular investigations are required to better characterize the specific influence of D-Asp-dependent JNK phosphorylation in modulating pro-death or pro-survival signaling. Remarkably, in line with *in vitro* study, we also reported that abnormally high levels of D-Asp in *Ddo*$^{-/-}$ mice are associated with a striking, time-dependent change in JNK phosphorylation in the mouse cortex.

Overstimulation of NMDARs is considered the main triggering event for developing a toxic condition that leads to cell death (Hardingham and Bading, 2003; Waxman and Lynch, 2005). Specifically, the activation of JNK signaling is intimately connected to NMDAR activity either at the postsynaptic site, where JNK promotes proapoptotic signaling activation (Centeno et al., 2007), or at the presynaptic site, where JNK has been seen to support the NMDAR-evoked release of glutamate (Rane et al., 1989). Corresponding to this knowledge, the pronounced changes in JNK phosphorylation observed in the cortex of *Ddo*$^{-/-}$ mice nicely mirror the severe dysfunctional NMDAR transmission, neuroinflammation, and cell death found in the cortical tissue of these mutants at 6 months of age (Cristino et al., 2015; Punzo et al., 2016).

The dysfunctional NMDAR neurotransmission found in adult *Ddo*$^{-/-}$ brain, by eliciting oxidative stress conditions (Punzo et al., 2016), might explain the massive increase in protein SUMOylation (Bondy and LeBel, 1993; Nicholls, 2004; Salim, 2017; Skaper et al., 1999) reported in cortical lysates of mutants at 2, 6, and 15 months of age. Protein SUMOylation is indeed highly activated during oxidative stress (Feligioni and Nistico, 2013) and this cellular mechanism has recently been linked to several brain pathological conditions, including Alzheimer's disease (Dangoumau et al., 2013; Eckermann, 2013; Marcelli et al., 2017). However, based on the recent finding by Feligioni and colleagues indicating that JNK signaling affects the SUMOylation process (Feligioni et al., 2011), we cannot exclude that abnormally increased levels of JNK phosphorylation in the *Ddo*$^{-/-}$ cortex might contribute to the higher protein SUMOylation observed in mutants.

Changes in Tau protein phosphorylation are associated with neuronal cell death (Canu et al., 1998; Mills et al., 1998) and Alzheimer's disease (Li et al., 2007). Previous studies revealed that Tau phosphorylation can be affected by NMDAR activation, oxidative stress, increased protein SUMOylation, and JNK phosphorylation (Alavi Naini and Soussi-Yanicostas, 2015; Allyson et al., 2010; De Montigny et al., 2013; Fleming and Johnson, 1995; Li et al., 2014; Luo et al., 2014; Ploia et al., 2011; Takahashi et al., 2008; Vogel et al., 2009; Xu et al., 2015; Yoshida et al., 2004; Zambrano et al., 2004). Interestingly, we found that altered JNK phosphorylation and protein SUMOylation are associated with extensive Tau hypophosphorylation at PHF1 and AT8 sites in the PFC and hippocampus of elderly *Ddo*$^{-/-}$ mice. Moreover, we demonstrated in primary cortical neurons that D-Asp induces, in a dose-dependent manner, MK801-sensitive changes in Tau phosphorylation at the same sites analyzed in *Ddo*$^{-/-}$ cortex. Taken together, our observations agree with previous studies demonstrating that activation of NMDAR induced Tau hypophosphorylation (Allyson et al., 2010; De Montigny et al., 2013; Fleming and Johnson, 1995; Halpain and Greengard, 1990) and support our previous observations demonstrating that glutamatergic neurotransmission at NMDAR sites is profoundly altered in *Ddo*$^{-/-}$ brains during aging (Errico et al., 2011a).

Tau phosphorylation is regulated by the opposing activities of kinases and phosphatases (Avila, 2008; Wang et al., 2007). Here, we found that hypophosphorylation of Tau protein cannot be ascribed to decreased activity of the main Tau kinases, GSK-3β, Cdk5, or ERK1/2 (Dolan and Johnson, 2010), in 15-month-old mutants since these kinases were phosphorylated at levels equivalent to those of wild-type mice, nor could they be attributed to decreased activity of JNK kinase, which is actually highly phosphorylated in the mutant mice. Phosphorylation of Akt was slightly reduced in the mutant mice, but this was unlikely to contribute directly to the observed tau hypophosphorylation, as this kinase does not modify Tau protein at the AT8, AT270, and PHF1 sites (Ksiezak-Reding et al., 2003).

Overall, these results suggest that modulation of one or more Tau phosphatases may underlie the changes seen in the *Ddo*$^{-/-}$ mice. Among the Tau phosphatases (Liu et al., 2005), the Ca^{2+}-calmodulin–dependent serine/threonine protein phosphatase calcineurin, also known as PP2B, is a strong candidate as it is activated upon NMDAR stimulation (Alagarsamy et al., 2005) and is involved in NMDAR-induced dephosphorylation of Tau (Fleming and Johnson, 1995; Halpain and Greengard, 1990). Further studies will be required to investigate the involvement of calcineurin and of other phosphatases such as PP2A and PP1 in regulating Tau phosphorylation in *Ddo*$^{-/-}$ mouse brain. Tau dephosphorylation has been reported to be associated with neuronal apoptosis (Amadoro et al., 2004; Canu et al., 1998; Kerokoski et al., 2001; Liu et al., 2010; Mills et al., 1998; Pristera et al., 2013; Rametti et al., 2004), oxidative stress (Ko et al., 1997) and glutamate-induced cell death (Lorio et al., 2001). In this latter case, Tau is also cleaved to a fragment (Lorio et al., 2001) like that seen in 100 μM D-Asp-treated primary cortical neurons. Based on these similarities, we argue that the Tau hypophosphorylation found in primary cortical neurons and in the cortex and hippocampus of *Ddo*$^{-/-}$ mice most likely reflects the cell death process activated by high levels of D-Asp.

APP and its proteolytic products are implicated in both normal nervous system function and Alzheimer's disease pathogenesis (Selkoe and Hardy, 2016). APP processing and Aβ peptide production are promoted by factors including NMDAR activation (Bordji et al., 2010; Hoey et al., 2009), JNK activation (Mazzitelli et al., 2011; Triaca et al., 2016), and cell death (Fiorelli et al., 2013), which are all biochemical and cerebral features of *Ddo*$^{-/-}$ aged brain. Interestingly, we observed increased age-dependent cortical immunostaining of APP in neuron cell soma of these mutants. The greater accumulation of APP may reflect altered APP trafficking, which could activate amyloidogenic APP processing (Wang et al., 2017), but we did not find any accumulation of Aβ40 and Aβ42 peptides in the PFC and hippocampus of *Ddo*$^{-/-}$ mice. In line with a recent finding reporting that D-Asp is able to counteract Aβ accumulation in a mouse model of neuropathic pain (D'Aniello et al., 2017), our data indicate that an abnormally high D-Asp level does not increase amyloidogenic processing of APP during aging.

In line with the lack of an evident link between abnormally high D-Asp levels in *Ddo*$^{-/-}$ mice and the appearance of molecular AD-like hallmarks (*i.e.*, increased Tau phosphorylation and increased Aβ peptides), HPLC and qPCR performed on human samples did not reveal any significant variations in D-Asp and *DDO* mRNA levels, respectively, in the cortex of AD patients compared to nondemented individuals *post-mortem*, thus suggesting that D-Asp metabolism is unaltered in a cortical region critically affected by AD. However, further studies with larger samples size are mandatory to clarify this issue, since other groups

reported altered D-Asp levels in the *post mortem* brain of AD patients (D'Aniello et al., 1998; Fisher et al., 1991).

In conclusion, our data confirm a fundamental neuroprotective role of DDO activity in adult mammalian brain and, in turn, demonstrate for the first time that abnormally high D-Asp concentrations induce neurotoxicity by activating NMDAR-mediated pro-death signaling pathway. In the light of this work, it is tempting to speculate that some neurodegenerative forms of precocious brain aging and dementia could be linked to genetic mutations in *DDO* that, through the inactivation of DDO and the corresponding upregulation of D-Asp levels, might enhance NMDAR-dependent neurodegenerative processes and apoptotic cell death. Nevertheless, alterations in D-Asp content do not seem to produce the classical neurodegenerative features observed in Alzheimer's disease. Indeed, neither β-amyloid alterations nor Tau hyperphosphorylation occurs in the PFC of $Ddo^{-/-}$ mice. In agreement with these findings, our clinical observations displayed unaltered D-Asp and *DDO* mRNA changes in the cortex of AD patients. Therefore, future studies are required to better clarify the involvement of dysfunctional D-Asp metabolism in neurodegenerative diseases.

Acknowledgements

Postmortem human brain samples were provided by the Netherlands Brain Bank (NBB) (Netherlands Institute for Neuroscience, Amsterdam). NC was supported by 2017 ANVUR – FFABR (Finanziamento delle Attività Base di Ricerca). AU was supported by a grant from Fondazione Cariplo. We thank Maria Teresa Ciotti for assistance with the primary cortical cultures and Alessia Casamassa for critical discussion.

Declaration of interest

None.

References

Alagarsamy, S., Saugstad, J., Warren, L., Mansuy, I.M., Gereau, R.W.T., Conn, P.J., 2005. NMDA-induced potentiation of mGluR5 is mediated by activation of protein phosphatase 2B/calcineurin. Neuropharmacology 49 (Suppl. 1), 135–145.

Alavi Naini, S.M., Soussi-Yanicostas, N., 2015. Tau hyperphosphorylation and oxidative stress, a critical vicious circle in neurodegenerative Tauopathies? Oxidative Med. Cell. Longev. 2015, 151979.

Allyson, J., Dontigny, E., Auberson, Y., Cyr, M., Massicotte, G., 2010. Blockade of NR2A-containing NMDA receptors induces tau phosphorylation in rat hippocampal slices. Neural Plast. 2010, 340168.

Amadoro, G., Serafino, A.L., Barbato, C., Ciotti, M.T., Sacco, A., Calissano, P., Canu, N., 2004. Role of N-terminal tau domain integrity on the survival of cerebellar granule neurons. Cell Death Differ. 11, 217–230.

Amadoro, G., Ciotti, M.T., Costanzi, M., Cestari, V., Calissano, P., Canu, N., 2006. NMDA receptor mediates tau-induced neurotoxicity by calpain and ERK/MAPK activation. Proc. Natl. Acad. Sci. U. S. A. 103, 2892–2897.

Augustinack, J.C., Schneider, A., Mandelkow, E.M., Hyman, B.T., 2002. Specific tau phosphorylation sites correlate with severity of neuronal cytopathology in Alzheimer's disease. Acta Neuropathol. 103, 26–35.

Avila, J., 2008. Tau kinases and phosphatases. J. Cell. Mol. Med. 12, 258–259.

Bessero, A.C., Chiodini, F., Rungger-Brandle, E., Bonny, C., Clarke, P.G., 2010. Role of the c-Jun N-terminal kinase pathway in retinal excitotoxicity, and neuroprotection by its inhibition. J. Neurochem. 113, 1307–1318.

Bifulco, D., Pollegioni, L., Tessaro, D., Servi, S., Molla, G., 2013. A thermostable L-aspartate oxidase: a new tool for biotechnological applications. Appl. Microbiol. Biotechnol. 97, 7285–7295.

Bondy, S.C., LeBel, C.P., 1993. The relationship between excitotoxicity and oxidative stress in the central nervous system. Free Radic. Biol. Med. 14, 633–642.

Bordji, K., Becerril-Ortega, J., Nicole, O., Buisson, A., 2010. Activation of extrasynaptic, but not synaptic, NMDA receptors modifies amyloid precursor protein expression pattern and increases amyloid-ss production. J. Neurosci. 30, 15927–15942.

Borsello, T., Croquelois, K., Hornung, J.P., Clarke, P.G., 2003. N-methyl-d-aspartate-triggered neuronal death in organotypic hippocampal cultures is endocytic, autophagic and mediated by the c-Jun N-terminal kinase pathway. Eur. J. Neurosci. 18, 473–485.

Burd, J.F., Usategui-Gomez, M., 1973. A colorimetric assay for serum lactate dehydrogenase. Clin. Chim. Acta 46, 223–227.

Canu, N., Dus, L., Barbato, C., Ciotti, M.T., Brancolini, C., Rinaldi, A.M., Novak, M., Cattaneo, A., Bradbury, A., Calissano, P., 1998. Tau cleavage and dephosphorylation in cerebellar granule neurons undergoing apoptosis. J. Neurosci. 18, 7061–7074.

Centeno, C., Repici, M., Chatton, J.Y., Riederer, B.M., Bonny, C., Nicod, P., Price, M., Clarke, P.G., Papa, S., Franzoso, G., Borsello, T., 2007. Role of the JNK pathway in NMDA-mediated excitotoxicity of cortical neurons. Cell Death Differ. 14, 240–253.

Colombo, A., Bastone, A., Ploia, C., Sclip, A., Salmona, M., Forloni, G., Borsello, T., 2009. JNK regulates APP cleavage and degradation in a model of Alzheimer's disease. Neurobiol. Dis. 33, 518–525.

Cristino, L., Luongo, L., Squillace, M., Paolone, G., Mango, D., Piccinin, S., Zianni, E., Imperatore, R., Iannotta, M., Longo, F., Errico, F., Vescovi, A.L., Morari, M., Maione, S., Gardoni, F., Nistico, R., Usiello, A., 2015. D-aspartate oxidase influences glutamatergic system homeostasis in mammalian brain. Neurobiol. Aging 36, 1890–1902.

Dangoumau, A., Veyrat-Durebex, C., Blasco, H., Praline, J., Corcia, P., Andres, C.R., Vourc'h, P., 2013. Protein SUMOylation, an emerging pathway in amyotrophic lateral sclerosis. Int. J. Neurosci. 123, 366–374.

D'Aniello, A., Lee, J.M., Petrucelli, L., Di Fiore, M.M., 1998. Regional decreases of free D-aspartate levels in Alzheimer's disease. Neurosci. Lett. 250, 131–134.

D'Aniello, A., Luongo, L., Romano, R., Iannotta, M., Marabese, I., Boccella, S., Belardo, C., de Novellis, V., Arra, C., Barbieri, A., D'Aniello, B., Scandurra, A., Magliozzi, L., Fisher, G., Guida, F., Maione, S., 2017. D-aspartic acid ameliorates painful and neuropsychiatric changes and reduces beta-amyloid Abeta1-42 peptide in a long lasting model of neuropathic pain. Neurosci. Lett. 651, 151–158.

De Montigny, A., Elhiri, I., Allyson, J., Cyr, M., Massicotte, G., 2013. NMDA reduces tau phosphorylation in rat hippocampal slices by targeting NR2A receptors, GSK3beta, and PKC activities. Neural Plast. 2013, 261593.

Dolan, P.J., Johnson, G.V., 2010. The role of tau kinases in Alzheimer's disease. Curr. Opin Drug Discov. Dev. 13, 595–603.

Eckermann, K., 2013. SUMO and Parkinson's disease. NeuroMolecular Med. 15, 737–759.

Errico, F., Nistico, R., Palma, G., Federici, M., Affuso, A., Brilli, E., Topo, E., Centonze, D., Bernardi, G., Bozzi, Y., D'Aniello, A., Di Lauro, R., Mercuri, N.B., Usiello, A., 2008. Increased levels of d-aspartate in the hippocampus enhance LTP but do not facilitate cognitive flexibility. Mol. Cell. Neurosci. 37, 236–246.

Errico, F., Nistico, R., Napolitano, F., Mazzola, C., Astone, D., Pisapia, T., Giustizieri, M., D'Aniello, A., Mercuri, N.B., Usiello, A., 2011a. Increased D-aspartate brain content rescues hippocampal age-related synaptic plasticity deterioration of mice. Neurobiol. Aging 32, 2229–2243.

Errico, F., Nistico, R., Napolitano, F., Oliva, A.B., Romano, R., Barbieri, F., Florio, T., Russo, C., Mercuri, N.B., Usiello, A., 2011b. Persistent increase of D-aspartate in D-aspartate oxidase mutant mice induces a precocious hippocampal age-dependent synaptic plasticity and spatial memory decay. Neurobiol. Aging 32, 2061–2074.

Esposito, S., Pristera, A., Maresca, G., Cavallaro, S., Felsani, A., Florenzano, F., Manni, L., Ciotti, M.T., Pollegioni, L., Borsello, T., Canu, N., 2012. Contribution of serine racemase/d-serine pathway to neuronal apoptosis. Aging Cell 11, 588–598.

Fagg, G.E., Matus, A., 1984. Selective association of N-methyl aspartate and quisqualate types of L-glutamate receptor with brain postsynaptic densities. Proc. Natl. Acad. Sci. U. S. A. 81, 6876–6880.

Feligioni, M., Nistico, R., 2013. SUMO: a (oxidative) stressed protein. NeuroMolecular Med. 15, 707–719.

Feligioni, M., Brambilla, E., Camassa, A., Sclip, A., Arnaboldi, A., Morelli, F., Antoniou, X., Borsello, T., 2011. Crosstalk between JNK and SUMO signaling pathways: deSUMOylation is protective against H2O2-induced cell injury. PLoS One 6, e28185.

Fiorelli, T., Kirouac, L., Padmanabhan, J., 2013. Altered processing of amyloid precursor protein in cells undergoing apoptosis. PLoS One 8, e57979.

Fisher, G.H., D'Aniello, A., Vetere, A., Padula, L., Cusano, G.P., Man, E.H., 1991. Free D-aspartate and D-alanine in normal and Alzheimer brain. Brain Res. Bull. 26, 983–985.

Fleming, L.M., Johnson, G.V., 1995. Modulation of the phosphorylation state of tau in situ: the roles of calcium and cyclic AMP. Biochem. J. 309 (Pt 1), 41–47.

Guida, F., Luongo, L., Marmo, F., Romano, R., Iannotta, M., Napolitano, F., Belardo, C., Marabese, I., D'Aniello, A., De Gregorio, D., Rossi, F., Piscitelli, F., Lattanzi, R., de Bartolomeis, A., Usiello, A., Di Marzo, V., de Novellis, V., Maione, S., 2015. Palmitoylethanolamide reduces pain-related behaviors and restores glutamatergic synapses homeostasis in the medial prefrontal cortex of neuropathic mice. Mol Brain 8, 47.

Hall, A.M., Roberson, E.D., 2012. Mouse models of Alzheimer's disease. Brain Res. Bull. 88, 3–12.

Halpain, S., Greengard, P., 1990. Activation of NMDA receptors induces rapid dephosphorylation of the cytoskeletal protein MAP2. Neuron 5, 237–246.

Hardingham, G.E., Bading, H., 2003. The Yin and Yang of NMDA receptor signalling. Trends Neurosci. 26, 81–89.

Hashimoto, A., Kumashiro, S., Nishikawa, T., Oka, T., Takahashi, K., Mito, T., Takashima, S., Doi, N., Mizutani, Y., Yamazaki, T., et al., 1993. Embryonic development and postnatal changes in free D-aspartate and D-serine in the human prefrontal cortex. J. Neurochem. 61, 348–351.

Hoey, S.E., Williams, R.J., Perkinton, M.S., 2009. Synaptic NMDA receptor activation stimulates alpha-secretase amyloid precursor protein processing and inhibits amyloid-beta production. J. Neurosci. 29, 4442–4460.

Homma, H., 2007. Biochemistry of D-aspartate in mammalian cells. Amino Acids 32, 3–11.

Jong, Y.J., Kumar, V., O'Malley, K.L., 2009. Intracellular metabotropic glutamate receptor 5 (mGluR5) activates signaling cascades distinct from cell surface counterparts. J. Biol. Chem. 284, 35827–35838.

Kerokoski, P., Suuronen, T., Salminen, A., Soininen, H., Pirttila, T., 2001. The levels of cdk5 and p35 proteins and tau phosphorylation are reduced during neuronal apoptosis. Biochem. Biophys. Res. Commun. 280, 998–1002.

Ko, L., Odawara, T., Yen, S.H., 1997. Menadione-induced tau dephosphorylation in cultured human neuroblastoma cells. Brain Res. 760, 118–128.

Krashia, P., Ledonne, A., Nobili, A., Cordella, A., Errico, F., Usiello, A., D'Amelio, M., Mercuri, N.B., Guatteo, E., Carunchio, I., 2016. Persistent elevation of D-aspartate enhances NMDA receptor-mediated responses in mouse substantia nigra pars

compacta dopamine neurons. Neuropharmacology 103, 69–78.
Ksiezak-Reding, H., Pyo, H.K., Feinstein, B., Pasinetti, G.M., 2003. Akt/PKB kinase phosphorylates separately Thr212 and Ser214 of tau protein in vitro. Biochim. Biophys. Acta 1639, 159–168.
Laemmli, U.K., 1970. Cleavage of structural proteins during the assembly of the head of bacteriophage T4. Nature 227, 680–685.
Li, B., Chohan, M.O., Grundke-Iqbal, I., Iqbal, K., 2007. Disruption of microtubule network by Alzheimer abnormally hyperphosphorylated tau. Acta Neuropathol. 113, 501–511.
Li, K., Jia, H., She, X., Cui, B., Zhang, N., Chen, X., Xu, C., An, G., Ma, Q., 2014. Role of NMDA receptors in noise-induced tau hyperphosphorylation in rat hippocampus and prefrontal cortex. J. Neurol. Sci. 340, 191–197.
Liu, J., Lin, A., 2005. Role of JNK activation in apoptosis: a double-edged sword. Cell Res. 15, 36–42.
Liu, F., Grundke-Iqbal, I., Iqbal, K., Gong, C.X., 2005. Contributions of protein phosphatases PP1, PP2A, PP2B and PP5 to the regulation of tau phosphorylation. Eur. J. Neurosci. 22, 1942–1950.
Liu, X.A., Liao, K., Liu, R., Wang, H.H., Zhang, Y., Zhang, Q., Wang, Q., Li, H.L., Tian, Q., Wang, J.Z., 2010. Tau dephosphorylation potentiates apoptosis by mechanisms involving a failed dephosphorylation/activation of Bcl-2. J. Alzheimers Dis. 19, 953–962.
Lorio, G., Avila, J., Diaz-Nido, J., 2001. Modifications of tau protein during neuronal cell death. J. Alzheimers Dis. 3, 563–575.
Luo, H.B., Xia, Y.Y., Shu, X.J., Liu, Z.C., Feng, Y., Liu, X.H., Yu, G., Yin, G., Xiong, Y.S., Zeng, K., Jiang, J., Ye, K., Wang, X.C., Wang, J.Z., 2014. SUMOylation at K340 inhibits tau degradation through deregulating its phosphorylation and ubiquitination. Proc. Natl. Acad. Sci. U. S. A. 111, 16586–16591.
Marcelli, S., Ficulle, E., Iannuzzi, F., Kovari, E., Nistico, R., Feligioni, M., 2017. Targeting SUMO-1ylation contrasts synaptic dysfunction in a mouse model of Alzheimer's disease. Mol. Neurobiol. 54, 6609–6623.
Mazzitelli, S., Xu, P., Ferrer, I., Davis, R.J., Tournier, C., 2011. The loss of c-Jun N-terminal protein kinase activity prevents the amyloidogenic cleavage of amyloid precursor protein and the formation of amyloid plaques in vivo. J. Neurosci. 31, 16969–16976.
McKhann, G., Drachman, D., Folstein, M., Katzman, R., Price, D., Stadlan, E.M., 1984. Clinical diagnosis of Alzheimer's disease: report of the NINCDS-ADRDA work group under the auspices of Department of Health and Human Services Task Force on Alzheimer's disease. Neurology 34, 939–944.
Milde, S., Adalbert, R., Elaman, M.H., Coleman, M.P., 2015. Axonal transport declines with age in two distinct phases separated by a period of relative stability. Neurobiol. Aging 36, 971–981.
Mills, J.C., Lee, V.M., Pittman, R.N., 1998. Activation of a PP2A-like phosphatase and dephosphorylation of tau protein characterize onset of the execution phase of apoptosis. J. Cell Sci. 111 (Pt 5), 625–636.
Mitchell, S.J., Scheibye-Knudsen, M., Longo, D.L., de Cabo, R., 2015. Animal models of aging research: implications for human aging and age-related diseases. Ann. Rev. Anim. Biosci. 3, 283–303.
Molla, G., Porrini, D., Job, V., Motteran, L., Vegezzi, C., Campaner, S., Pilone, M.S., Pollegioni, L., 2000. Role of arginine 285 in the active site of Rhodotorula gracilis D-amino acid oxidase. A site-directed mutagenesis study. J. Biol. Chem. 275, 24715–24721.
Monahan, J.B., Michel, J., 1987. Identification and characterization of an N-methyl-D-aspartate-specific L-[3H]glutamate recognition site in synaptic plasma membranes. J. Neurochem. 48, 1699–1708.
Nicholls, D.G., 2004. Mitochondrial dysfunction and glutamate excitotoxicity studied in primary neuronal cultures. Curr. Mol. Med. 4, 149–177.
Nistico, R., Florenzano, F., Mango, D., Ferraina, C., Grilli, M., Di Prisco, S., Nobili, A., Saccucci, S., D'Amelio, M., Morbin, M., Marchi, M., Mercuri, N.B., Davis, R.J., Pittaluga, A., Feligioni, M., 2015. Presynaptic c-Jun N-terminal kinase 2 regulates NMDA receptor-dependent glutamate release. Sci. Rep. 5, 9035.
Nuzzo, T., Sacchi, S., Errico, F., Keller, S., Palumbo, O., Florio, E., Punzo, D., Napolitano, F., Copetti, M., Carella, M., Chiariotti, L., Bertolino, A., Pollegioni, L., Usiello, A., 2017. Decreased free d-aspartate levels are linked to enhanced d-aspartate oxidase activity in the dorsolateral prefrontal cortex of schizophrenia patients. NPJ Schizophr. 3, 16.
Ogita, K., Yoneda, Y., 1988. Disclosure by triton X-100 of NMDA-sensitive [3H] glutamate binding sites in brain synaptic membranes. Biochem. Biophys. Res. Commun. 153, 510–517.
Olverman, H.J., Jones, A.W., Mewett, K.N., Watkins, J.C., 1988. Structure/activity relations of N-methyl-D-aspartate receptor ligands as studied by their inhibition of [3H] D-2-amino-5-phosphonopentanoic acid binding in rat brain membranes. Neuroscience 26, 17–31.
Ploia, C., Antoniou, X., Sclip, A., Grande, V., Cardinetti, D., Colombo, A., Canu, N., Benussi, L., Ghidoni, R., Forloni, G., Borsello, T., 2011. JNK plays a key role in tau hyperphosphorylation in Alzheimer's disease models. J. Alzheimers Dis. 26, 315–329.
Pristera, A., Saraulli, D., Farioli-Vecchioli, S., Strimpakos, G., Costanzi, M., di Certo, M.G., Cannas, S., Ciotti, M.T., Tirone, F., Mattei, E., Cestari, V., Canu, N., 2013. Impact of N-tau on adult hippocampal neurogenesis, anxiety, and memory. Neurobiol. Aging 34, 2551–2563.
Punzo, D., Errico, F., Cristino, L., Sacchi, S., Keller, S., Belardo, C., Luongo, L., Nuzzo, T., Imperatore, R., Florio, E., De Novellis, V., Affinito, O., Migliarini, S., Maddaloni, G., Sisalli, M.J., Pasqualetti, M., Pollegioni, L., Maione, S., Chiariotti, L., Usiello, A., 2016. Age-related changes in D-aspartate oxidase promoter methylation control extracellular D-aspartate levels and prevent precocious cell death during brain aging. J. Neurosci. 36, 3064–3078.
Rametti, A., Esclaire, F., Yardin, C., Terro, F., 2004. Linking alterations in tau phosphorylation and cleavage during neuronal apoptosis. J. Biol. Chem. 279, 54518–54528.
Rane, S.G., Walsh, M.P., McDonald, J.R., Dunlap, K., 1989. Specific inhibitors of protein kinase C block transmitter-induced modulation of sensory neuron calcium current. Neuron 3, 239–245.
Ransom, R.W., Stec, N.L., 1988. Cooperative modulation of [3H]MK-801 binding to the N-methyl-D-aspartate receptor-ion channel complex by L-glutamate, glycine, and polyamines. J. Neurochem. 51, 830–836.
Sacchi, S., Lorenzi, S., Molla, G., Pilone, M.S., Rossetti, C., Pollegioni, L., 2002. Engineering the substrate specificity of D-amino-acid oxidase. J. Biol. Chem. 277, 27510–27516.
Sacchi, S., Novellis, V., Paolone, G., Nuzzo, T., Iannotta, M., Belardo, C., Squillace, M., Bolognesi, P., Rosini, E., Motta, Z., Frassineti, M., Bertolino, A., Pollegioni, L., Morari, M., Maione, S., Errico, F., Usiello, A., 2017. Olanzapine, but not clozapine, increases glutamate release in the prefrontal cortex of freely moving mice by inhibiting D-aspartate oxidase activity. Sci. Rep. 7, 46288.
Salim, S., 2017. Oxidative stress and the central nervous system. J. Pharmacol. Exp. Ther. 360, 201–205.
Schell, M.J., Cooper, O.B., Snyder, S.H., 1997. D-aspartate localizations imply neuronal and neuroendocrine roles. Proc. Natl. Acad. Sci. U. S. A. 94, 2013–2018.
Selkoe, D.J., Hardy, J., 2016. The amyloid hypothesis of Alzheimer's disease at 25 years. EMBO Mol. Med. 8, 595–608.
Skaper, S.D., Floreani, M., Ceccon, M., Facci, L., Giusti, P., 1999. Excitotoxicity, oxidative stress, and the neuroprotective potential of melatonin. Ann. N. Y. Acad. Sci. 890, 107–118.
Stankovic-Valentin, N., Drzewicka, K., Konig, C., Schiebel, E., Melchior, F., 2016. Redox regulation of SUMO enzymes is required for ATM activity and survival in oxidative stress. EMBO J. 35, 1312–1329.
Takahashi, K., Ishida, M., Komano, H., Takahashi, H., 2008. SUMO-1 immunoreactivity co-localizes with phospho-tau in APP transgenic mice but not in mutant tau transgenic mice. Neurosci. Lett. 441, 90–93.
Tare, M., Modi, R.M., Nainaparampil, J.J., Puli, O.R., Bedi, S., Fernandez-Funez, P., Kango-Singh, M., Singh, A., 2011. Activation of JNK signaling mediates amyloid-ss-dependent cell death. PLoS One 6, e24361.
Thomas, G.M., Lin, D.T., Nuriya, M., Huganir, R.L., 2008. Rapid and bi-directional regulation of AMPA receptor phosphorylation and trafficking by JNK. EMBO J. 27, 361–372.
Triaca, V., Sposato, V., Bolasco, G., Ciotti, M.T., Pelicci, P., Bruni, A.C., Cupidi, C., Maletta, R., Feligioni, M., Nistico, R., Canu, N., Calissano, P., 2016. NGF controls APP cleavage by downregulating APP phosphorylation at Thr668: relevance for Alzheimer's disease. Aging Cell 15, 661–672.
Van Veldhoven, P.P., Brees, C., Mannaerts, G.P., 1991. D-aspartate oxidase, a peroxisomal enzyme in liver of rat and man. Biochim. Biophys. Acta 1073, 203–208.
Vogel, J., Anand, V.S., Ludwig, B., Nawoschik, S., Dunlop, J., Braithwaite, S.P., 2009. The JNK pathway amplifies and drives subcellular changes in tau phosphorylation. Neuropharmacology 57, 539–550.
Wang, J.Z., Grundke-Iqbal, I., Iqbal, K., 2007. Kinases and phosphatases and tau sites involved in Alzheimer neurofibrillary degeneration. Eur. J. Neurosci. 25, 59–68.
Wang, X., Zhou, X., Li, G., Zhang, Y., Wu, Y., Song, W., 2017. Modifications and trafficking of APP in the pathogenesis of Alzheimer's disease. Front. Mol. Neurosci. 10, 294.
Waxman, E.A., Lynch, D.R., 2005. N-methyl-D-aspartate receptor subtypes: multiple roles in excitotoxicity and neurological disease. Neuroscientist 11, 37–49.
Xu, C.S., Liu, A.C., Chen, J., Pan, Z.Y., Wan, Q., Li, Z.Q., Wang, Z.F., 2015. Overactivation of NR2B-containing NMDA receptors through entorhinal-hippocampal connection initiates accumulation of hyperphosphorylated tau in rat hippocampus after transient middle cerebral artery occlusion. J. Neurochem. 134, 566–577.
Yoshida, H., Hastie, C.J., McLauchlan, H., Cohen, P., Goedert, M., 2004. Phosphorylation of microtubule-associated protein tau by isoforms of c-Jun N-terminal kinase (JNK). J. Neurochem. 90, 352–358.
Zambrano, C.A., Egana, J.T., Nunez, M.T., Maccioni, R.B., Gonzalez-Billault, C., 2004. Oxidative stress promotes tau dephosphorylation in neuronal cells: the roles of cdk5 and PP1. Free Radic. Biol. Med. 36, 1393–1402.